Health Physics Vol. 46, No. 4 (April), pp. 891 914, 1984
Printed in the U.S.A.

0017-9078/84 $3.00 + .00
Pergamon Press Ltd.

FLUENCE TO DOSE EQUIVALENT CONVERSION FACTORS CALCULATED WITH EGS3 FOR ELECTRONS FROM 100 keV TO 20 GeV AND PHOTONS FROM 11 keV TO 20 GeV

D. W. O. ROGERS
Physics Division, National Research Council of Canada, Ottawa, Canada K1A 0R6

(*Received* 12 *October* 1982; *accepted* 13 *June* 1983)

Abstract—The EGS3 Monte-Carlo electron-photon transport simulation package has been used to calculate dose equivalent per unit fluence vs depth curves for broad parallel beams of mono-energetic electrons, positrons and photons incident on a 30-cm-thick slab of ICRU four-element tissue. The electron kinetic energy range covered is 100 keV to 20 GeV and that for photons is 11 keV to 20 GeV. It was found that by making minor modifications, EGS3 is in reasonable agreement with other codes for electron energies down to 100 keV. Complete dose equivalent vs depth curves as a function of electron and photon energy are presented to allow proper calculations of the maximum dose equivalent for a mixed photon and electron spectrum since there are substantial variations in the locations of the peak dose equivalent. Explicit calculations demonstrate that $1/r^2$ corrections give an accurate means to convert results for broad parallel beams to those for point source geometries. The relative contributions of various physical processes to the peak dose equivalent are presented.

1. INTRODUCTION

THE BIOLOGICAL effects of radiation incident on the human body are very complicated. In both radiation protection and medical therapy situations, it is common practice to simplify the situation and quantify the radiation field and the biological risk associated with it in terms of the quantity dose equivalent which is usually numerically equal to the absorbed dose to tissue for photons and electrons. The advantage of this simplification is that absorbed dose to tissue is a well defined physical quantity (energy deposited per unit mass) which can be measured or deduced in a variety of ways. In radiation protection situations it sometimes occurs that the measured quantity is particle fluence and hence a set of conversion factors is needed to transform the measured fluence to the required quantity, namely dose equivalent. A further simplification often employed for radiation protection purposes is to associate the biological risk with the peak value of the dose equivalent in the body. Proper assessment of this peak value from the measured fluence spectrum requires knowledge of dose equivalent vs depth curves as a function of particle energy. This paper reports a series of calculations which provide the factors to enable this conversion to be made for electrons or photons over the entire energy range of practical interest. Both electrons and photons are dealt with because the transport of these particles in a material is strongly coupled. Incident photons set electrons in motion and at energies above a few MeV the resultant displacement has a major effect on the distribution of dose equivalent. Conversely, an incident electron produces bremsstrahlung photons which, at higher energies contribute a significant fraction of the dose equivalent at the peak.

EGS3 is a general purpose Monte-Carlo electron–photon transport simulation package developed at SLAC by Ford and Nelson (Fo78; Ne80). Because of its flexibility it is being used at the National Research Council of Canada (NRCC) in a wide variety of radiation protection and medical dosimetry-related problems.

The present study was undertaken for two purposes. One was to investigate the accuracy of EGS3 at low electron and photon energies. The

N.R.C.C. 22777

physical models used in the simulation package are thought to become less accurate for electron energies below about 1 MeV and for photon simulations in which fluorescent x rays are important ($\leqslant$ 100 keV). However, these restrictions do not appear to be significant in energy deposition problems in tissue or water down to incident electron energies of 100 keV or photon energies down to 11 keV. The second purpose of this study was to generate a set of fluence to maximal dose equivalent conversion factors and a complete set of depth-dose curves for monoenergetic electron and photon beams to be used to calculate depth-dose curves for arbitrary spectra calculated or measured in other situations. Throughout this paper the maximal dose equivalent is defined as the peak value of the dose equivalent for broad parallel beams of radiation incident normally on a 30-cm-thick slab of ICRU four-element tissue. Because of the large differences in depth-dose shapes, knowledge of the entire depth-dose curve is essential if the maximal dose equivalent for a spectrum is to be determined.

The next section presents a brief overview of the EGS3 simulation package, the data used in these calculations and the user code written for these calculations. Section 3 presents the results and compares them to those obtained previously. Section 4 discusses the influence of a change from a broad parallel beam geometry to a beam from a point source. The last section presents a separation of the dose equivalent at the peak into its various components. The Appendix presents a set of depth-dose curves for protons and electrons.

The unit used for dose equivalent is the sievert (1 Sv = 100 rem) and that for absorbed dose is the gray (1 Gy = 100 rad). The dose equivalent in Sv is considered to be numerically equal to the absorbed dose to tissue in Gy, although there is some evidence that this is not the case for low-energy photons (ICRU29). The notation 6.5E-5 stands for 6.5×10^{-5}.

2. THE CALCULATIONS

2.1 *The* EGS3 *code*

The calculations have been done using the EGS3 Monte-Carlo simulation package which is described in detail in Fo78 and Ne80. A brief description has appeared in Ro82 which also describes several minor errors in EGS3 which have been corrected at NRCC. For some of the high-energy cases studied here, it was also necessary to make a minor modification to several EGS3 subroutines to ensure $\cos\theta \leqslant 1$. The code considers all physical processes believed to be important in the transport of electrons or positrons above 1 MeV or photons above the K edge. In photon transport, the code considers Compton scattering (Klein–Nishina cross section applied to free electrons), pair production (with an approximate treatment of triplet production), and the photoelectric effect (photoelectrons are tracked but K x rays and Auger electrons are considered to be deposited locally). Cross sections from Storm and Israel are used (St70) except for pair-production cross sections above about 50 MeV where theoretical estimates are used. Electron-positron transport is simulated using the condensed history technique with energy-loss fluctuations accounted for through the random nature of the elastic scattering events. Bremsstrahlung production, positron annihilation in flight, elastic Moller and Bhabha scattering from electrons and Moliere multiple-scattering from atomic nuclei are all taken into account. The approximations used for the photoelectric events determine the low-energy cutoff for photon transport but this is not expected to be a significant shortcoming in tissue where the highest K x ray has an energy well below 10 keV. As has been shown elsewhere (Ro83) if the default step-size algorithm in the EGS3 system is modified (e.g. to give a 4% energy loss per step), then, at the cost of greatly increased computing time, low-energy electron transport simulations with EGS3 give accurate results.

In the final stages of this work, a minor error in EGS3 was found. Correcting the error increases multiple scattering for low-energy electrons. This has 20% effect on the peak of the 100-keV depth dose curve and virtually no effect on the depth-dose curves for incident electrons with energies above 2 MeV. The results presented for electrons with incident energies below 10 MeV were computed with the NRCC's corrected version of EGS3 and this correction will be reflected in EGS4 which will be released by SLAC.

2.2 *The NRCC user's code*

An EGS3 user code called DOSE2 was developed for these calculations. It considers a semi-infinite plate of arbitrary material which can be broken up into any number of regions along the depth axis. Energy deposition can also be recorded as a function of radius but radial regions are not employed. Incident electrons, positrons or photons can be considered for broad parallel beams, finite parallel beams or collimated isotropic sources. The broad parallel beam case is accomplished by considering an incident pencil beam and scoring the total energy deposited per unit areal density in semi-infinite slabs at each depth. Air effects are not considered.

Although it appears to underestimate them, the statistical uncertainties were estimated by doing all calculations in 10 batches and computing the rms variation on the average. In general, results presented for peaks on depth-dose curves have a statistical uncertainty of less than 1% to ensure that uncertainties in the physical input data are the dominant source of uncertainty in the final results. It should be noted that a small bias towards high values is introduced in choosing the peak value of the dose equivalent because the maximum value is selected from several bins which often have nearly equal values. This biasing was always less than 1%.

A small modification to the EGS3 package has been made to allow for an exponential transformation of photon pathlengths. This variance reduction technique proves useful where a biasing towards events at shallow depths improves the information on the buildup region. Careful optimization has not been done but efficiency has been increased by a factor of 2–3 in several cases. Biasing is only done for forward going photons. For $\cos\theta \geqslant 0$ (where θ is the Z direction cosine with the Z axis being the depth axis), the number of mean free paths is chosen as

$$\mathrm{MFP} = -B \cdot \ln R_i$$

$$B = 1./(1. - \mathrm{C} \cdot \cos\theta)$$

and the weight is changed to

$$\mathrm{WT}' = \mathrm{WT} \cdot B \cdot \mathrm{e}^{-MFP \cdot C \cdot \cos\theta},$$

where C is an input variable ranging from 0 (no effect) to -4 (shorten an initial pathlength by a factor of 5) and R_i is a random number distributed uniformly on the interval (0, 1).

2.3 *The cross section data and parameters*

The slab was considered to be standard 4-element unit density tissue as defined by the ICRU (i.e. in *ICRU Report* 19—H, 10.1% by weight; C, 11.1%; N, 2.6%; O, 76.2%). Calculations were also done with water as the phantom material to compare to previous calculations.

Figure 1 presents a summary of the photon cross section data as used by the EGS3 system. Note the 3.5% discontinuity in the gamma mean free path at 50 MeV which occurs because the data of Storm and Israel (St70) are used for the pair production cross sections below 50 MeV and a different normalization is used above this. This discontinuity leads to a corresponding discontinuity in the calculated fluence to maximal dose equivalent conversion factor for photons at 50 MeV.

The corresponding input electron cross-section data is somewhat more difficult to summarize because in various energy regions data sets were used corresponding to different energy cutoffs. Let [AE, AP] denote a data set for which all electrons with total energy less than AE keV (kinetic energy = AE-511) and photons with energy less than AP keV are considered to deposit their energy locally. All electron inter-

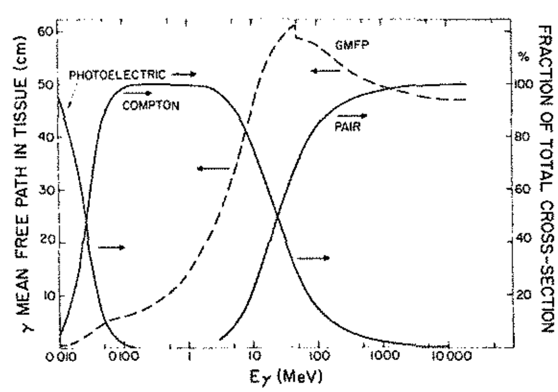

FIG. 1. Photon cross sections for ICRU tissue as prepared by PEGS3 for use by EGS3. The gamma mean free path between interactions is shown on the left scale and the fractions of the total cross section given by photoelectric, Compton and pair production processes are given by the right-hand scale. The 3% discontinuity in the cross section at 50 MeV is the result of a problem matching pair production normalization factors.

actions which create scattered electrons with energies less than AE keV or bremsstrahlung photons with energy less than AP keV are treated as part of a continuous energy loss mechanism. Figure 2 presents restricted stopping powers for electrons in tissue for two sets of energy cutoffs as well as the unrestricted stopping power (for e^- in muscle from Be64). Electrons continuously lose energy as they slow down and they can also lose energy via discrete events, either elastic scattering from electrons with both resulting electrons having energy above AE or by bremsstrahlung emission of a photon with energy above AP. Figure 3 presents the mean free path of electrons between such discrete events. The discontinuity in these curves occurs at the threshold for elastic scattering (at $511 + 2 \times (\text{AE} - 511)$ keV). The curve with AE = 521 is far below the energy range for which EGS3 was intended. The fact that the electron mean free path does not increase monotonically as the electron energy decreases means that EGS3 does not properly handle the change in cross section as the electron loses energy during each step. However no effects of this problem have been noted, especially since the continuous energy loss mechanisms dominate in the regions where the changing cross section might have an effect.

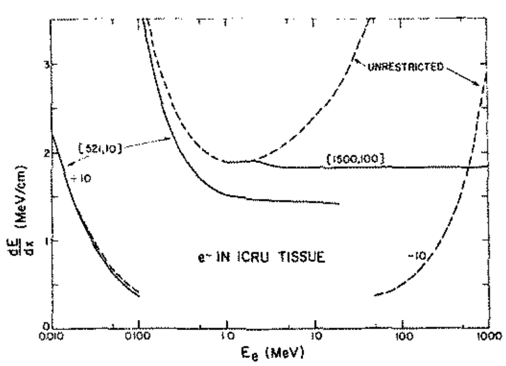

FIG. 2. The restricted electron stopping powers in tissue for the two sets of cutoffs used for these calculations. The notation [AE, AP] means the stopping power includes only those interactions creating electrons with total energies less than AE keV or photons with energies less than AP keV. The restricted stopping powers were computed by the PEGS3 part of the EGS3 system.

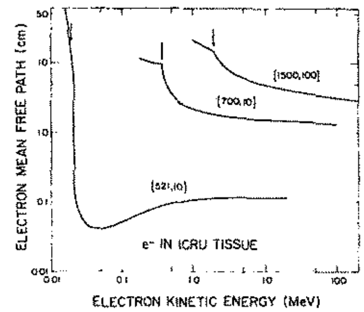

FIG. 3. Electron mean free paths in ICRU tissue between discrete interactions in which either knock-on electrons with total energies above AE keV or bremsstrahlung photons with energies above AP keV are created. The arrows denote the threshold energy for the production of knock-on electrons for that particular data set. The values were calculated by PEGS3.

The parameters to be set for each run are: ECUT, PCUT, the electron and photon energy cutoffs; AE & AP, the cutoffs in the input data set; ESTEPE, the fractional energy loss per step in electron transport; *C*, the exponential path-length transformation variable (for initial photons only); the number of histories to follow; and the widths of depth bins. The last three were set arbitrarily to ensure adequate statistics and depth resolution. ESTEPE was only used with incident electrons since the EGS3 default step-size algorithm was adequate for incident photons. The value of ESTEPE was chosen by decreasing it at several benchmark energies to find the largest value below which a change of less than 2% was observed in the peak dose value. The choice of values for ECUT was considerably more difficult and is discussed in Section 3.3. Note that run times per history can vary by over an order of magnitude depending on the choices of ESTEPE, AE and AP. Tables 1 and 2 summarize the parameters used although these are presented as a matter of record rather than as an indication of optimized choices.

2.4 *Normalization of results*

The results are quoted in terms of dose equivalent per unit incident fluence. Fluence takes into account the angle of incidence and, with the

Table 1. EGS3 parameter values used for electron depth-dose calculations

Energy Range	Cutoffs (keV)[1] Electron	Photon	ESTEPE[2]	# histories	VAX CPU Time(s)
100 → 900 keV	521	10	0.04	10,000	800 → 2400
1 → 10 MeV	711	10	0.04	10,000	600 → 2600
20 → 50 MeV	1500	100	-	10,000	450 → 1000
70 → 20,000 MeV	1500	100	-	4,000	500 → 1700

[1]User cutoffs ECUT using [521, 10] or [1500, 100] data sets.

[2]The default electron step-size algorithm in EGS3 has been modified to change TMXS such that the continuous energy loss in each step is a set fraction, ESTEPE, of the electron kinetic energy, see Ro83.

Table 2. EGS3 parameter values used for photon depth-dose calculations

Photon Energy Range	Cutoff (keV)[1] Electron	Photon	C[2]	# histories $\div 10^3$	VAX CPU Time 10^3s
11 → 600 keV	521	10	0	400	2 → 27
0.8 → 10 MeV	700	10	-3	300	10 → 41
20 → 20,000 MeV	1500	100	-1.5	80 → 2	0.7 → 8

[1]User cutoffs using [521, 10] or [1500, 100] data sets as appropriate.

[2]Exponential pathlength transformation variable – not optimized.

exception of a normally incident beam, it is not given by the number of incident particles divided by the area. For a point isotropic source D cm from a flat phantom, collimated to a finite solid angle Ω, the incident on-axis fluence for N histories is given by

$$\phi_o = \frac{N}{\Omega D^2},$$

where $\Omega = 4\pi(1-\gamma_o)/2$ is the solid angle subtended and γ_o is cosine of the maximum angle allowed by the collimator.

To compare the present results to some of the previous work and to experimental data, it is essential to know the conversion factors from fluence to exposure for photons below 10 MeV. The collision kerma K_c for a medium (to be distinguished from the total kerma; see At79) is given by

$$K_c = 1.602 \times 10^{-10} E_\gamma \phi \frac{\mu_{en}}{\rho} \quad [\mathrm{Gy}], \qquad (1)$$

where E_γ is the photon energy in MeV; ϕ is the photon fluence in γ/cm^2; and μ_{en}/ρ is the mass energy-absorption coefficient in cm^2/g for the medium.

It should be noted that under conditions of charged-particle equilibrium, the collision kerma equals the absorbed dose to the medium and hence equation (1) is often used as a formula for the absorbed dose. Exposure X is defined as

$$\begin{aligned} X &= K_c\Big|_{\mathrm{air}} \frac{e}{\bar{W}}\Big|_{\mathrm{air}} && [\mathrm{C/kg}] \\ &= 4.740 \times 10^{-12} E_\gamma \phi \frac{\mu_{en}}{\rho}\Big|_{\mathrm{air}} && [\mathrm{C/kg}] \\ &= 1.837 \times 10^{-8} E_\gamma \phi \frac{\mu_{en}}{\rho}\Big|_{\mathrm{air}} && [\mathrm{R}], \qquad (2) \end{aligned}$$

where use is made of the fact that $1\ \mathrm{R} = 2.58 \times 10^{-4}$ C/kg (exactly) and the best estimate of $e/\bar{W}$ is 1/33.8 C/J where $\bar{W}$, the average energy to create an ion pair in dry air, is 33.8 eV/ion pair as recommended in *ICRU Report* 31. Another quantity frequently introduced in these types of calculations is the absorbed dose to air (more properly the air collision kerma) which is given by

$$K_c\Big|_{\text{air}} = X\frac{\bar{W}}{e}\Big|_{\text{air}} \qquad \text{[J/kg]}$$
$$= 0.00872X \qquad \text{[J/kg = Gy to air]},$$

where X is in R.

Table 3 presents conversion factors based on equation (2) and Hubbell's mass energy absorption coefficients (Hu77; these differ from values in Hu69 by $\leq 1\%$ except at 30 keV, and agree with Storm and Israel's values). At most energies, these values are within 2% of the values given in *ICRP Report* 21. Table 3 also presents the conversion factors used by Dimbylow and Francis (Di79) which differ by -6% to $+8\%$. The choice of these conversion factors is important for experimental comparison purposes but are an unnecessary complication in presenting the Monte-Carlo results which compute dose equivalent per unit fluence. To convert to dose equivalent per unit exposure, one should use Column 2 of Table 3.

3. RESULTS

This section presents the calculated fluence to maximal dose equivalent conversion factors. The present results are shown in Fig. 4. The fluence is that incident on the slab. This conversion factor is conceptually different from the dose equivalent index which is defined as the peak value of the dose equivalent in a 30-cm diam. sphere of ICRU tissue. More notably, at least when non-parallel beams are used, fluence to dose equivalent index conversion factors refer to the fluence at the location of the center of the

Table 3. Conversion factors from fluence to exposure in dry air using $\bar{W}$ = 33.8 eV/ion pair and mass energy-absorption coefficient from Hubbell (1977) compared to those used by Dimbylow and Francis (1979). Conversion factors from fluence to absorbed dose to air (more properly the air collision kerma) are given by multiplying Column 2 by 0.00872 Gy to air/R. Here, and in all other tables, the exponent in the second column applies to the other columns as well

E_γ MeV	R.cm² Present	R.cm² Di79	Difference %
0.01	8.54 E-10	8.06	-5.6
0.015	3.59 E-10	3.38	-5.9
0.02	1.94 E-10	1.83	-5.4
0.03	8.29 E-11	8.00	-3.5
0.04	4.93 E-11	4.72	-4.2
0.05	3.71 E-11	3.58	-3.5
0.06	3.32 E-11	3.29	-0.8
0.08	3.52 E-11	3.61	2.5
0.10	4.26 E-11	4.42	3.7
0.15	6.88 E-11	7.19	4.6
0.2	9.82 E-11	10.3	4.9
0.3	1.58 E-10	1.65	4.2
0.4	2.17 E-10	2.25	3.8
0.5	2.73 E-10	2.82	3.5
0.6	3.25 E-10	3.39	4.2
0.8	4.24 E-10	4.41	4.1
1.0	5.12 E-10	5.35	4.5
1.25	6.11 E-10	6.31	3.2
1.5	7.02 E-10	7.30	4.1
2.0	8.61 E-10	8.93	3.7
3.0	1.18 E-9	1.19	5.1
4.0	1.37 E-9	1.45	5.6
5.0	1.60 E-9	1.69	5.8
6.0	1.82 E-9	1.93	6.3
8.0	2.24 E-9	2.39	6.8
10.0	2.66 E-9	2.87	8.1
20.0	4.80 E-9	-	-

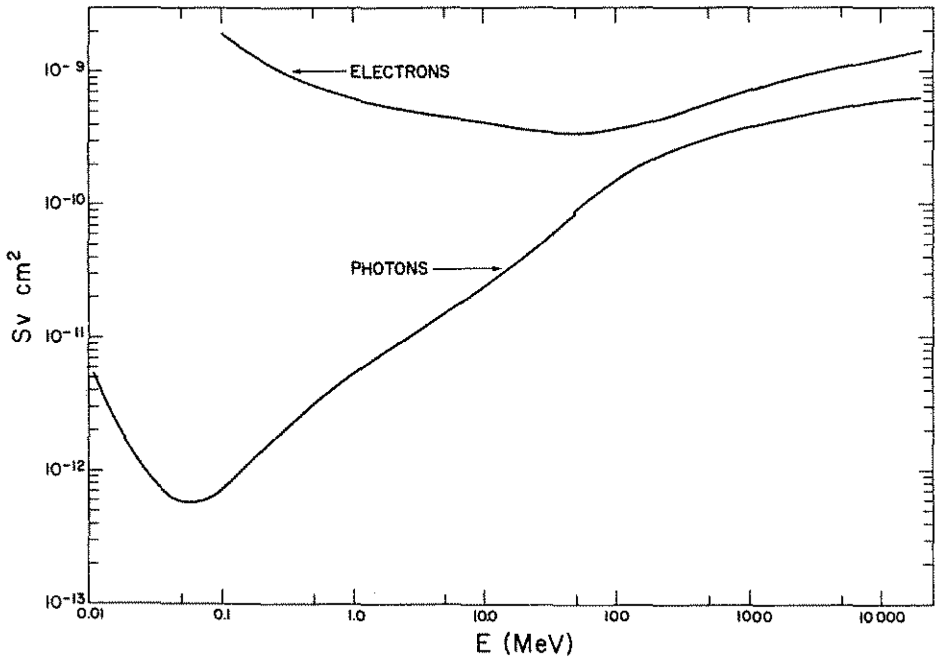

FIG. 4. A summary of the fluence to maximal dose equivalent conversion factors calculated in this work for broad parallel beams of electrons or photons incident normally on a 30-cm-thick slab of ICRU tissue. The 3% discontinuity in the photon values reflect the discontinuity in the cross section data presented in Fig. 1.

sphere when the sphere is absent. As will be seen below, these distinctions are not very important for parallel beams but they can be significant in practice.

3.1 *Photon results below* 10 *MeV*

Table 4 summarizes the present calculated photon fluence to maximal dose equivalent conversion factors over the energy range 10 keV to 10 MeV for broad parallel beams of photons incident on a 30-cm-thick semi-infinite slab of ICRU four-element tissue. Table 4 and Fig. 5 also present comparisons to a wide range of other calculations, each of which are discussed briefly.

3.1.1 *Nelson and Chilton.* Very close agreement is obtained with the results in Ne82, which is gratifying since the geometry and tissue material are identical and similar processes are considered in the Monte-Carlo calculations.

3.1.2 *Trubey/ANSI.* Claiborne and Trubey's (Cl70) combined discrete ordinate and Monte-Carlo results for photons on the 11-element Oak Ridge National Laboratory (ORNL) tissue were the basis of the ANSI recommended conversion factors (AN77). These results have been further refined by Tapia and Trubey (Ta80) below 1 MeV using Monte-Carlo calculations. Below 300 keV, even these later results (Ta80) are significantly larger than the EGS3 results reported here. Nelson and Chilton's work suggests these differences are almost entirely due to the different tissue compositions. Even small amounts of heavier elements cause a significant increase in the photon cross section because the cross section for the photo-electric effect, which dominates at these low energies, varies as $Z^{3.5}$ (Hu69). In as much as tissue does contain these heavier elements and since Tapia and Trubey's results are more conservative, their values should be used for photons with energies below

Table 4. Photon fluence to maximal dose equivalent conversion factors in Sv · cm² for broad parallel beams of photons with energies between 10 keV and 10 MeV incident on various phantoms (described in the text). The present results are for a semi-infinite, 30-cm-thick slab of four-element ICRU tissue

	Sv.cm²						
E_γ MeV	Present[1]	Dimbylow & Francis[2] Di79	Hohlfeld & Grosswendt[3] Ho82	Tapia & Trubey Ta80	ANSI -Trubey AN77	ICRP21[4]	Nelson & Chilton[5] Ne82
0.010	5.40 E-12[6])	-	7.18	9.31	9.42	7.67	6.85
0.015	2.97 E-12	-	3.35	4.06	5.42	3.08	3.02
0.020	1.68 E-12	1.76*(5)	2.03	2.29	3.28	1.64	1.71
0.030	8.83 E-13	9.10 (21)	10.3	11.4	16.2	7.16	8.97
0.040	6.55 E-13	6.45 (21)	7.01	7.78	10.0	4.34	6.54
0.050	5.86 E-13	5.40 (22)	5.82	6.83	8.06	3.36	5.99
0.060	5.76 E-13	5.18 (17)	5.38	6.50	7.33	3.08	5.64
0.080	6.27 E-13	5.60 (16)	5.52	6.78	7.25	3.36	6.28
0.100	7.33 E-13	6.33 (31)	6.28	7.75	7.86	4.10	7.28
0.150	-	9.40 (38)	9.12	-	10.5	6.66	
0.200	1.39 E-12	1.28 (6)	1.22	-	1.39	0.95	
0.300	2.03 E-12	1.92 (9)	1.82	2.03	2.11	1.53	
0.400	2.63 E-12	2.43 (10)	2.38	2.61	2.74	2.10	
0.500	3.18 E-12	3.02 (10)	2.90	3.14	3.19	2.64	
0.600	3.65 E-12	3.58 (9)	3.37	3.67	3.78	3.16	
0.800	4.66 E-12	4.60 (9)	4.33	4.58	4.67	4.11	
1.0	5.49 E-12	5.58 (9)	5.18	5.42	5.50	4.95	
1.5	[7])	7.20 (8)	6.98	-		6.78	
2.0	8.73 E-12	9.23 (16)	8.56	-	8.90	8.33	
3.0	1.13 E-11	1.20 (2)	1.11	-	1.16	1.09	
4.0	1.35 E-11	1.40 (2)	1.35	-	1.40	1.32	
5.0	1.55 E-11	1.61 (2)	1.56	-	1.62	1.53	
6.0	1.73 E-11	1.81*(2)	1.78	-	1.83	1.73	
7.0	1.91 E-11	2.03*(2)		-	2.03		
8.0	2.10 E-11	2.21*(2)	2.19	-	2.24	2.13	
10.0	2.43 E-11	2.61*(2)	2.60	-	2.65	2.52	

[1]Statistical uncertainties <1% in all cases.

[2]Obtained by converting data tabulated in Di79 from Sv/Gy to air to Sv.cm² using the data presented in Table 3 and then doing a log-log interpolation. Data is the maximum value in a 30 cm diameter ICRU-tissue sphere. Values shown with an * do not occur on the central axis. Value in brackets is the statistical uncertainty in the last digit.

[3]Obtained by digitizing graphical data in Ho82 and converting it from Sv/Gy to air to Sv.cm² using conversion factors in col 2 of Table 3. Data is the maximum value in a 30 cm diameter ICRU-tissue sphere.

[4]ICRP21 presents the collision kerma in water as defined in eq'n 1.

[5]Statistical uncertainties <3%.

[6]Value at 11 keV.

[7]Value for ^{60}Co, E = 1.250 MeV is 6.42×10^{-12}.

300 keV. Above 300 keV, the present results agree well with the ORNL values up to several MeV. In the energy region above this, the present values are consistently lower because the effects of electron transport become important. When electron transport is ignored in EGS3, for 10-MeV photons the maximal dose equivalent conversion factor is 2.62×10^{-11} Sv · cm², in good agreement with Claiborne and Trubey's value.

3.1.3 *ICRP Report* 21. For photons with energies below 10 MeV, the ICRP values are based on a collision kerma-to-water approximation to the maximal dose equivalent (see equation (1)). This approximation ignores electron transport, photon scattering and attenuation, and recapture of bremsstrahlung photons. Above 3 MeV these effects appear to cancel each other out and the approximation is remarkably accurate. However the approxi-

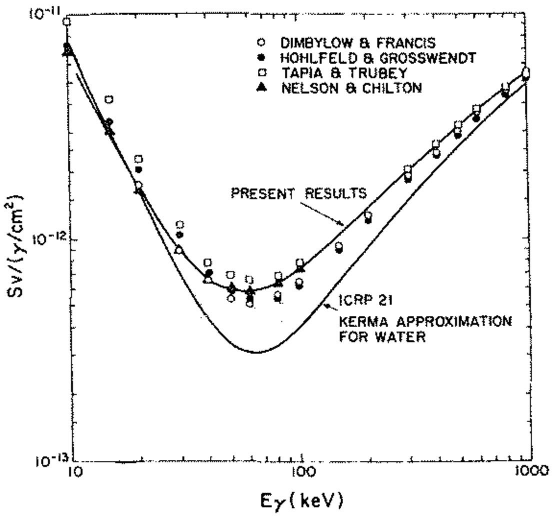

FIG. 5. A comparison of the present calculations to previous calculations for photons in the energy range 10–1000 keV. The results of Dimbylow and Francis, and Hohlfeld and Grosswendt are for a 30-cm spherical phantom and are thus not directly comparable to the other slab calculations. The major part of the difference with Tapia and Trubey arises because of their use of a more realistic tissue composition in which the trace elements play a significant role at these low energies.

mation gives a significant underestimate of the dose equivalent at lower energies, especially near 100 keV where scattered radiation produces a large fraction of the dose equivalent (see Section 5). This difference has significant implications for many dosimetry problems in which a ratio of mass energy absorption coefficients is used to transfer dose from one material to another.

3.1.4 *Dimbylov and Francis*; *Hohlfeld and Grosswendt*. These results are both Monte-Carlo calculations of the dose equivalent index for four-element ICRU tissue. Direct comparisons are somewhat difficult, especially for those energies at which the peak dose equivalent is off the central axis of the sphere. There is also some confusion about conversion factors from fluence to absorbed dose to air (see footnotes 2 and 3 of Table 4). In particular, the method adopted here is different from that used in Ho82 in as much as they compared their results in Sv/Gy to air directly to those of Di79 which implies they have used the same conversion factors for fluence to absorbed dose to air. The present comparison assumes different conversion factors were used in each case.

Overall, the agreement is satisfactory given the statistical uncertainties in the other calculations and the geometric differences. It is somewhat puzzling that Di79 which considered electron transport, and Ho82 and Cl70 which did not consider electron transport, all obtain essentially the same values at photon energies above 6 MeV.

3.2 *Photon results above* 10 *MeV*

Table 5 and Fig. 6 give the present results for the fluence to maximal dose equivalent conversion factors for broad parallel beams of photons with energies above 10 MeV and compares them to several previous results. All previous results are for a water slab but values calculated with EGS3 for a water slab were only slightly larger than for tissue ($\leqslant 5\%$ difference) and are not reported here. The discontinuity in the present results near 50 MeV reflects the discontinuity in the input cross section data discussed in Section 2.3.

ICRP Report 21 explicitly states (p. 15) that

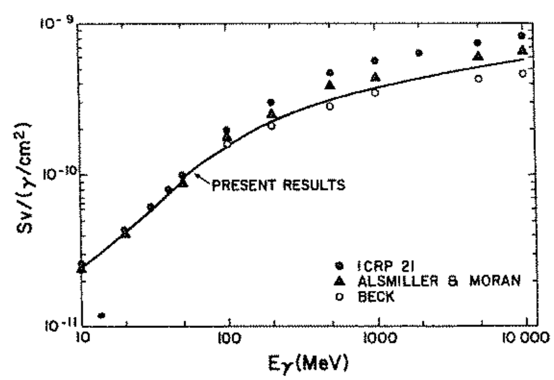

FIG. 6. A comparison of the present calculations to previous calculations for photons in the energy range 10 MeV to 10 GeV. The previous calculations were all for a water slab but the differences were found to be small. The data from Be70 and Al68 were for 5-cm or 7.5-cm bin widths and therefore should be increased slightly ($\approx 10\%$) for comparison purposes (see Table 5).

Table 5. Photon fluence to maximal dose equivalent conversion factors in Sv · cm² for broad parallel beams of photons with energies above 10-MeV incident on a 30-cm-thick semi-infinite slab of ICRU tissue or water

	Sv.cm²					
E_γ MeV	Present Peak[1]	5cm² bins[2]	ICRP21[3]	Water Collision Kerma[4]	Alsmiller & Moran[5]	Beck[5]
10	2.43 E-11		2.53	2.48	2.5	-
20	4.16 E-11		4.34	4.36[7]	4.2	-
30	5.77 E-11		6.30	6.30		-
40	7.32 E-11		8.17	8.20		-
47.5	8.36 E-11					-
50	9.25 E-11		9.92	10.1	8.9	-
55	9.78 E-11	-	-	-	-	-
100	1.53 E-10	1.52	1.98	1.99	1.8	1.6
200	2.27 E-10	2.20	3.02	-	2.6	2.1
500	3.18 E-10	2.94	4.79	-	3.9	2.9
1000	3.79 E-10	3.50	5.67	-	4.4	3.5
2000	4.35 E-10	3.86	6.46	-	-	-
5000	5.21 E-10	4.77	7.51[6]	-	6.1[6]	4.4[6]
10000	5.77 E-10	5.14	8.17	-	6.7	4.7
20000	6.19 E-10	5.63	8.68	-	7.2	5.1

[1]Statistical uncertainty <1%.

[2]Average dose equivalent to the 5cm bin surrounding the peak. For comparison to the other high energy calculations which were done for 5 cm bins.

[3]ICRP21 states these values are based on the work of Alsmiller & Moran, increased from the 5 cm bin calculations to estimate the peak value. However, below 100 MeV it appears to be based on the Water Collision Kerma values (as done below 10 MeV).

[4]Eq'n 1 using the mass energy-absorption coefficients of Hu69.

[5]Tabulated values from Al68 and Be70 for maximum value of average absorbed dose to water in 7.5 and 5 cm wide bins irradiated by broad parallel beams of photons.

[6]Value for 5200 MeV.

[7]The value based on a more recent value of μ_{en}/ρ (Hu77) is 4.20×10^{-11} Sv.cm².

above 10 MeV its recommended conversion factors are based on the work of Alsmiller and Moran (Al68), but increased to estimate the peak value since the tabulated results in Al68 were for the average dose in 7.5-cm-wide bins. However, based on the comparison in Table 5, it appears that between 10 and 100 MeV the ICRP values are actually those given by the water collision kerma approximation, as was the case below 10 MeV.

Column 2 of Table 5 gives the average dose equivalent obtained in a 5-cm bin about the peak value for energies above 100 MeV. It shows the average value is 1–11% less than the peak value whereas *ICRP Report* 21 estimates of peak values were 16–45% greater than the average values. However, the present results are significantly lower than Alsmiller and Moran's values even taking this factor into account. This can be explained by the fact that they did not take into account the density effect correction for high-energy electron stopping powers. Especially below 1000 MeV, the present results for 5-cm bins are in excellent agreement with the calculation of Beck (Be70), who took the density effect into account.

3.3 *Electron results below* 100 *MeV*

The results for electrons below 10 MeV are quite sensitive to the electron energy cutoff and step-size parameters chosen for the calculations. For example, for 500-keV electrons, restricting the electron step-size to a 4% energy loss reduces the peak dose equivalent value by

10% compared to the result using the EGS3 default step-size. Also, for a given electron energy cutoff ECUT, the results can be sensitive to the value of the electron cutoff energy AE of the data set used. There is a complex interplay of effects which occurs. These are discussed in detail elsewhere (Ro83; Ro83b). The parameters in Table 1 were chosen by reducing the energy loss per step until no significant ($\leqslant \sim 1\%$) changes occurred and by using the highest values of AE and ECUT which did not introduce significant changes. The change to EGS3 mentioned in Section 2.1 had a distinct effect on the depth-dose curves for incident energies below 1 MeV. It also had a minor effect on parameter selection. However the original parameters have been retained and the effects will be discussed elsewhere.

The results are summarized and compared to previous calculations in Table 6. The agreement is generally satisfactory but there are small systematic differences between ETRAN and EGS3, especially when the entire depth-dose curve is considered.

Figure 7 presents a comparison of the entire depth-dose curves for broad parallel beams of 20-MeV electrons as calculated by three different codes. The agreement with Nahum's results is remarkable and occurs at other energies, but there is a slight difference compared to the ETRAN results. These differences are typical of those at other energies as well, but are insignificant for radiation protection purposes. These differences are discussed in detail elsewhere (Ro83b).

3.4 *Electron results above* 100 *MeV*

Table 7 and Fig. 8 compare the present results to previous work for electron beams above 100 MeV. The *ICRP Report* 21 values are based

Table 6. Electron fluence to maximal dose equivalent conversion factors in Sv · cm² for broad parallel beams of electrons with energies below 100-MeV incident on a 30-cm-thick semi-infinite slab of ICRU tissue or water

	Sv.cm²			
	Present			
E_e MeV	Tissue[1] (3)	H_2O[1] (3)	ICRP21[2]	Other[2]
0.100	1.92 E-9	1.94	1.72	1.80 CYLT[4]
0.200	1.23 E-9	1.22	1.07	
0.300	9.66 E-10			
0.400	8.29 E-10			
0.500	7.68 E-10	7.70	7.12	7.35 CYLT[4]
0.600	7.16 E-10			
0.700	6.63 E-10			
0.800	6.48 E-10			
0.900	6.35 E-10			
1.0	6.15 E-10	6.18	5.79	5.79 CYLT[4], 5.71 Be82
1.5	5.59 E-10			
2.0	5.33 E-10	5.31	5.05	
3.0	5.00 E-10	5.01	4.8	
4.0	4.77 E-10			
5.0	4.74 E-10	4.68	4.48	4.66 Na75, 4.40 CYLT[4] 4.42 Be82
7.0	4.41 E-10			
10	4.17 E-10	4.22	4.15	4.08 Be69,4.18Na75, 4.03 Be82
20	3.65 E-10	3.73	3.86	3.75 Be69,3.80Na75, 3.63 Be82
30	3.53 E-10	3.57		3.68 Na75, 3.43 Be82
40	3.49 E-10			3.37 Be82
50	3.52 E-10	3.56	3.86	3.38 Be82
70	3.57 E-10			
100	3.74 E-10	3.78	4.15	

[1]Statistical uncertainty <1%.
[2]For a water phantom.
[3]Using default parameter values specified in Table 1.
[4]Using an NRCC version of CYLTRAN (an extended ETRAN, see Ha76); uncertainty <±2%

Table 7. Electron fluence to maximal dose equivalent conversion factors in Sv · cm² for broad parallel beams of electrons with energies above 100-MeV incident on a 30-cm-thick semi-infinite slab of ICRU tissue or water

E_e MeV	Sv.cm² Present Tissue[1]	H2O Peak	H2O 5cm bin	ICRP[2]	Alsmiller[3] & Moran	Beck[3]
100	3.74 E-10	3.78	3.74	4.15[4]	4.44	3.67
200	4.26 E-10	4.50	4.26	5.14	5.28	4.19
500	5.84 E-10	5.99	5.87	7.72	6.94	5.69
1000	7.19 E-10	7.48	7.07	9.26	8.89	6.78
2000	8.48 E-10	-	-	11.1		
5000	1.03 E-9	1.09[5]	1.01[5]	1.32[5]	1.17[5]	0.88[5]
10000	1.21 E-9	1.27	1.17	1.54	1.36	0.94
20000	1.41 E-9	1.43	1.31	1.85	1.58	1.03

[1]Statistical uncertainty <1%.

[2]ICRP21 values for water based on an estimate of the peak dose from the 5 cm binned values in Al68.

[3]Tabulated values from Al68 and Be70 for 7.5 and 5 cm wide water bins respectively.

[4]Not based on Al68.

[5]E_e = 5.2 GeV.

on the peak values estimated from the values in Al68 for average absorbed dose to water in 7.5-cm bins. As pointed out in Section 3.2 for high-energy photons, the peak estimation technique overestimates the peak but does not account for all of the differences between the present results and those in *ICRP Report* 21 or Al68, where the density effect correction to the electron stopping powers was not used. As was the case for photons, the present results are in good agreement with Beck's values below 1000 MeV although the current results are 15–30% higher above that energy.

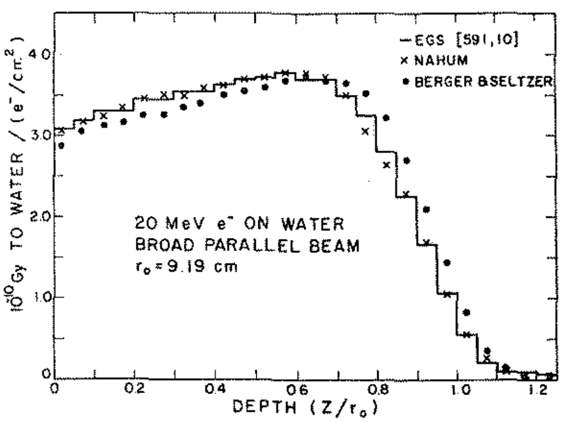

FIG. 7. A comparison of various calculations of the depth-dose curve for a broad parallel beam of 20-MeV electrons incident on a water phantom. The Berger and Seltzer results are from Be69 and those of Nahum from Na75.

3.5 *Positron results*

Positron depth-dose curves can be different from electron curves both because of the intrin-

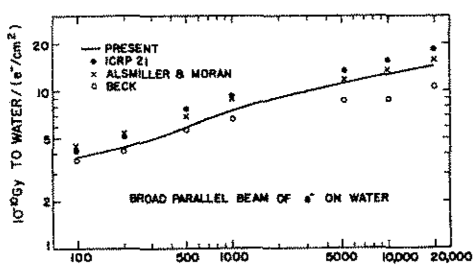

FIG. 8. A comparison of the present calculations to previous calculations of the maximal dose equivalent per unit incident fluence for broad parallel beams of electrons in the energy range 100 MeV to 20 GeV.

sically different scattering cross section (which is formally quite different from that for electrons for low energies) and because of the dose delivered by the pair of 511-keV photons created when the positrons annihilate.

This latter effect would not be important at higher energies where the majority of the positrons go through the slab. For lower energies, at depths greater than the positrons range, the effect does create a dose equivalent of the order of 1% of the peak dose equivalent.

Figure 9 shows the difference between the maximal dose equivalents for electrons and positrons. Despite the relatively large statistical uncertainty, it is clear that the net effect is for the positron values to be the same as the electron values except between roughly 5- and 100-MeV incident energies where they are about 5% lower. This difference can usually be ignored except for very precise work.

3.6 *Depth-dose curves*

The Appendix contains a complete set of depth vs dose equivalent curves for normally incident electrons and photons. These curves allow an estimate of the depth-dose equivalent curve to be made for an arbitrary incident spectrum of electrons and photons.

4. GEOMETRIC EFFECTS

The values presented in Section 3 refer to a broad parallel beam incident normally on a slab. In practice one often deals with an isotropic point source. The depth-dose curves and conversion factors in this case are given by

$$C_x(D) = C_{\parallel}(C) \cdot \left(\frac{x}{D + x}\right)^2,$$

where $C_x(D)$ is the dose equivalent at a depth of D cm, per unit incident on-axis fluence for an isotropic source x cm from the slab; and $C_{\parallel}(D)$ is the corresponding conversion factor for a broad parallel beam as found in the appendix. For a 7-MeV photon source, this relationship has been verified using the current Monte-Carlo code to hold to better than 2% for sources 30–100 cm from the slab.

Note that these point-source conversion factors are in terms of the incident on-axis fluence which, as discussed in Section 2.4, is not just the number of particles hitting the slab per unit area. Note also that both the parallel beam and point source factors apply to broad beams. Collimated beams will have somewhat reduced dose equivalent per unit fluence because of outscatter. The size of the reduction will depend on the relative importance of scatter contributions to the dose equivalent at a given location but, for example, the dose equivalent on axis in a parallel, 15-cm diam, 7-MeV photon beam is roughly 2–5% less than in a broad parallel beam.

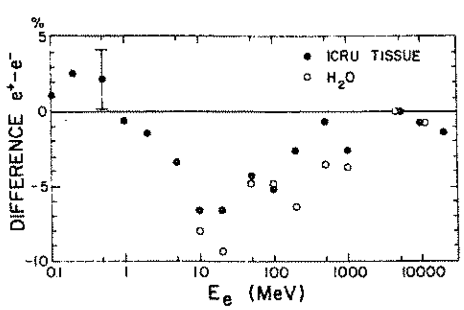

FIG. 9. The percentage difference between the maximal dose equivalent per unit incident fluence for broad parallel beams of e^+ and e^- incident on water and tissue phantoms. Despite rather larger statistical uncertainties, it is clear that the e^+ values are about 5% less than the e^- values between 5 and 100 MeV.

5. DOSE COMPONENTS

EGS3 has been modified at NRCC to pass an information word along with each particle. This feature makes it easy to score separately the contributions to the dose coming from different classes of events. A users code called SCATI has been written which does this at a cost of about 25% increase in computing time compared to DOSE2.

For incident photons, SCATI keeps track of the fraction of the dose due to electrons set in motion by (i) the photons of the primary beam; (ii) photons Compton scattered one, two or three times; (iii) photons interacting via pair production; and (iv) photons generated by bremsstrahlung emission and electrons set in motion by a previous interaction.

Note that these are not necessarily exclusive subsets. In particular, "pair" events can include "brem" events and vice versa.

For incident electrons, SCATI keeps track of the fraction of the dose due to (i) local energy loss by the primary electron via soft bremsstrahlung photons and knock-on electrons below the energy cutoffs (i.e. the restricted stopping power energy loss); (ii) knock-on electrons (with initial energy above the energy cutoffs); (iii) electrons which stop, i.e. fall below the energy cutoff; and (iv) electrons set in motion by bremsstrahlung generated photons.

Figures 10 and 11 present the relative contributions of the various dose components to the maximal dose equivalent as a function of incident photon and electron energy, respectively.

For 15-keV photons the majority of the peak dose is delivered via primary photons undergoing photoelectric interactions. Between 50 and 500 keV the fraction of the dose delivered by the primary photon beam decreases dramatically because multiple Compton scatterings become important. For 100-keV photons it was found that 4% of the peak dose was due to photons which had Compton-scattered 10 or more times. This occurs because (i) the Compton process predominates; (ii) the differential cross section is not strongly forward peaked; and (iii) the photon mean free path is relatively short ($\leqslant 6$ cm).

For photon energies above 1 MeV, the majority of the dose is once again delivered by the primary beam. Multiple Compton scattering decreases because the differential cross section becomes forward peaked and the mean free path becomes much longer. Therefore most Compton-scattered photons pass through the slab phantom and very few deposit energy near

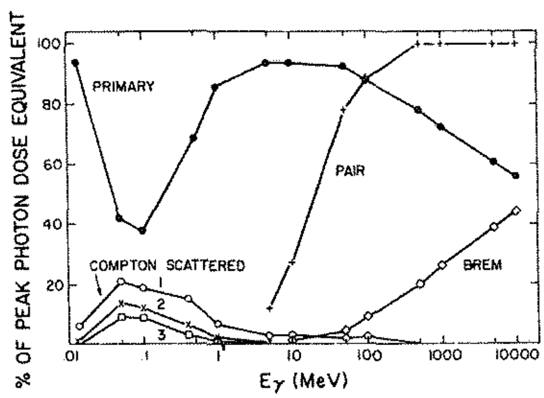

FIG. 10. The percentage contribution of various processes to the maximal dose equivalent per unit incident photon fluence as a function of photon energy. At 100 keV 4% of the peak dose is due to tenth order or higher Compton scatter events. The lines are visual guides only.

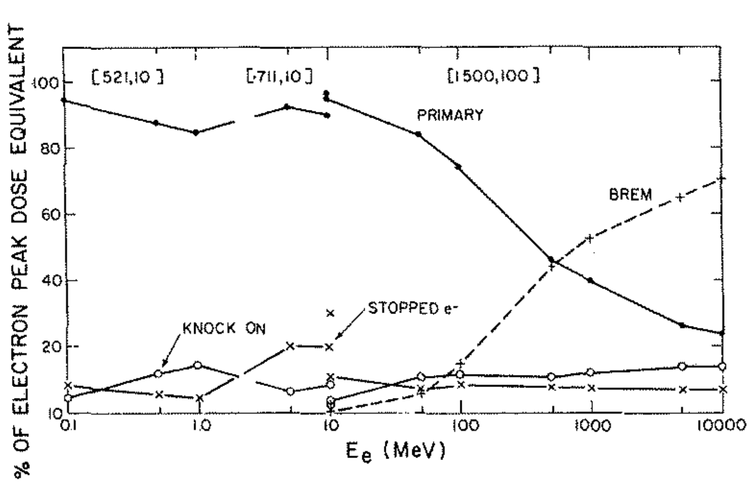

FIG. 11. The percentage contribution of various processes to the maximal dose equivalent per unit incident electron fluence conversion factors as a function of energy. The processes are defined in the text. The results are strong functions of the energy cutoffs used for the calculations. The cutoffs are indicated at the top of the figure. Three sets of calculations are presented at 10 MeV for the cases described in the text. The lines are visual guides only.

the peak at the front of the phantom. At 10 MeV and above, pair production begins to predominate and above 100 MeV a sizeable amount of the dose is delivered via bremsstrahlung emission since the radiation yield becomes substantial for the high-energy electrons generated in pair production events. The dose components presented in Fig. 10 are quite insensitive to the parameters chosen for the calculation.

In the case of electrons, the breakdown of the dose is highly dependent on the energy cutoffs used since the cutoff energy used for knock-on electrons clearly affects the division between knock-on and primary energy deposition. However the overall trends are still evident from Fig. 11. In particular, for energies below 100 MeV, the majority of the peak dose is due to local energy loss from the primary electron beam. To demonstrate the effects of energy cutoffs, three calculations were done with different energy cutoffs and/or data sets. In the terminology of Section 2.3, three cases were defined:

	ECUT	AE	PCUT	AP
Case A	1500	1500	100	100
Case B	1500	521	100	10
Case C	711	521	10	10

Case C corresponds to the values used for the 5-MeV point and Case A corresponds to the values used for the 50-MeV point. For a given value of AE the dose from stopped electrons will increase as ECUT is increased since higher energy electrons are considered stopped. Thus case B has a much higher stopped electron dose (30%) than Case C (20%). On the other hand, for a fixed ECUT the dose fraction due to stopped electrons will decrease as AE increases since fewer knock-on electrons are generated and allowed to stop (the energy is deposited as part of the continuous slowing down process instead). So Case A (AE = 1.5 MeV) has considerably fewer stopped electrons (11%) than Case B (AE = 521 keV, 30% stopped). As expected, the fraction of the dose from knock-on electrons decreases as ECUT increases since a larger fraction of the elastic scattering is considered part of the continuous slowing down process.

6. ACCURACY

The statistical uncertainty on the conversion factors was kept to less than $\pm 1\%$. In the worst case there may be a 1% bias towards high values because of selecting a maximum from several bins. Although coherent photon scattering may affect the very low-energy photon cases slightly, the EGS3 code in principle accounts for all major physical processes thought to be important for the energies concerned. For this reason these results are thought to be as accurate or more accurate than any of the previous calculations, many of which did not include all the effects handled by EGS3. There is some uncertainty introduced by parameter choice, especially for lower energy electron calculations. This uncertainty is thought to be less than 2%. There is also the uncertainty introduced by cross section data. The discontinuity in the photon data at 50 MeV indicates the uncertainty is at least of the order of 3% for higher energies although it is likely closer to 1% for lower energies where tabulated cross sections have been used. Uncertainties in the electron stopping powers are also of the order of 1–3% but the uncertainties in the maximal dose equivalent are not always sensitive to these values. The overall uncertainty in the calculation is therefore in the range 3–5%.

Experimental data are very hard to measure with an accuracy comparable to the uncertainty in these calculations. In a recent experiment using a carefully calibrated medical ion chamber in a nearly monoenergetic 7-MeV photon beam, the absorbed dose to water per unit fluence was found to be $1.2 \pm 3\%$ less than that calculated with EGS3 (Ma83).

As discussed in Section 3.1.2, the minor element constituents in tissue lead to a considerable increase in the calculated conversion factor below roughly 100 MeV. It is therefore advisable to use the results of Tapia and Trubey (Ta80) in this energy region.

The effect of photonuclear reactions have been ignored in these calculations although they do increase the photon cross-section by up to 3% near the giant resonance ($\sim 20 \rightarrow 25$ MeV). The calculations by Ing *et al.* (In82) of the integral absorbed dose of water from a 600 cm^2 beam of monoenergetic photons indicate that the photoneutrons contribute considerably less than 1% of the integral absorbed dose in the beam which suggests they will also have less than a 1% effect on the maximal dose equivalent values presented here.

7. SUMMARY

The fluence to dose equivalent conversion factors presented here provide a unified set of factors which apply to electrons and photons over the entire energy range of practical interest in radiation protection situations. By making minor modifications to EGS3 for low-energy electrons, it was found to be in reasonable agreement with previous calculations, thus giving confidence in the extension of its use to these low energies.

Acknowledgment—I would like to thank Ralph Nelson and his colleagues at the Stanford Linear Accelerator (SLAC) for their development of the EGS3 system which has made this work possible, and Alex Bielajew for useful discussions about the definition of fluence.

REFERENCES

Al68 Alsmiller R. G. and Moran H. S., 1968, "Dose Rate from High-Energy Electrons and Photons", *Nucl. Inst. & Meth.* **58**, 343.

AN77 American National Standards Institute/American Nuclear Society, 1977, "American National Standard Neutron and Gamma-Ray Flux-To-Dose-Rate Factors" ANSI, LaGrange Park, IL, Rep. ANSI/ANS-6.1.1—1977 (N666).

At79 Attix F. H., 1979, "The Partition of Kerma to Account for Bremsstrahlung", *Health Phys.* **36**, 347.

Be64 Berger M. J. and Seltzer S. M., 1964, "Tables of Energy Losses and Ranges of Electrons and Positrons", NASA, Washington, DC 20234, SP-3012.

Be69 Berger M. J. and Seltzer S. M., 1969, "Calculation of Energy and Charge Deposition and of the Electron Flux in a Water Medium Bombarded with 20 MeV Electrons", *Annals of the N.Y. Acad. Sci.* **161**, 8.

Be70 Beck H. L., 1970, "A New Calculation of Dose Rates from High Energy Electrons and Photons incident on 30 cm Water Slabs", *Nucl. Inst. & Meth.* **78**, 333.

Be82 Berger M. J. and Seltzer S. M., 1982 "Tables of Energy Deposition Distributions in Water Phantoms Irradiated by Point-Monodirectional Electron Beams with Energies from 1 to 60 MeV and Application to Broad Beams", National Bureau of Standards, Washington, DC 20234, Report NBSIR 82-2451.

Cl70 Claiborne H. C. and Trubey D. K., 1970, "Dose Rates in a Slab Phantom from Monoenergetic Gamma-rays", *Nucl. Appl. Tech.* 8, **450**.

Di79 Dimbylow P. J. and Francis T. M., "A Calculation of the Photon Depth-dose Distribution in the ICRU Sphere for a Broad Parallel Beam, a Point Source and an Isotropic Field", National Radiological Protection Board, Harwell, UK, NRPB-R92.

Fo78 Ford R. L. and Nelson W. R., 1978 "The EGS Code System", Stanford Linear Accelerator Center Stanford, CA, Report No. 210.

Ha76 Halbleib Sr. J. A., 1976, "CYLTRAN", *Nucl. Sci. Eng.* **61**, 288.

Ho82 Hohlfeld K. and Grosswendt B., 1982, "Conversion Factors for Determining Dose Equivalent Quantities from Absorbed Dose in Air for Photon Radiation", *Rad. Prot. Dosimetry* **1**, 277.

Hu69 Hubbell J. H., 1969, "Photon Cross Sections, Attenuation Coefficients and Energy Absorption Coefficients from 10 keV to 100 GeV", U.S. Dept. of Commerce, Washington, DC, Report NSRDS-NBS29.

Hu77 Hubbell J. H., 1977, "Photon Mass Attenuation and Mass Energy-Absorption Coefficients for H, C, N, O, Ar, and Seven Mixtures from 0.1 keV to 20 MeV", *Rad. Res.* **70**, 58.

Hu82 Hubbell J. H., 1982, "Photon Mass Attenuation and Energy-Absorption Coefficients from 1 keV to 20 MeV", *Int. J. of Appl. Radiat. Isot.* **33**, 1269.

In82 Ing H., Nelson W. R. and Shore R. A., 1982, "Unwanted Photon and Neutron Radiation Resulting from Collimated Photon Beams Interacting with the Body of Radiotherapy Patients", *Med. Phys.* **9**, 27.

ICRP71 International Commission on Radiological Protection, 1971, "Data for Protection Against Ionizing Radiation from External Sources" (Oxford: Pergamon Press).

ICRU71 International Commission on Radiation Units and Measurements, 1971, "Radiation Quantities and Units, *ICRU Report* 19 (Washington, DC: ICRU).

ICRU78 International Commission on Radiation Units and Measurements, 1978, "Dose Specification for Reporting External Beam Therapy with Photons and Electrons", *ICRU Report* 29 (Washington, DC: ICRU).

ICRU79 International Commission on Radiation Units and Measurements, 1979, "Average Energy Required to Produce an Ion Pair", *ICRU Report* 31 (Washington, DC: ICRU).

Ma83 Mach H. and Rogers D. W. O., 1983, "A Measurement of Absorbed Dose to Water per Incident 7 MeV Photon", National Research Council of Canada, Ottawa, to be published.

Na75 Nahum A. E., 1975, "Calculations of Electron Flux Spectra in Water Irradiated with Megvoltage Electron and Photon Beams with Applications to Dosimetry", Ph.D. Thesis. University of Edinburgh, Scotland.

Ne80 Nelson W. R. (Ed.), 1980, *Computer Techniques in Radiation Transport and Dosimetry* (New York: Plenum Press).

Ne82 Nelson R. F. and Chilton A. B., 1982, "Depth Doses for Low Energy Mono-energetic Photons", *Rad. Prot. Dosimetry* **1**, 285.

Ro82 Rogers D. W. O., 1982, "More Realistic Monte Carlo Calculations of Photon Detector Response Functions", *Nucl. Inst. & Meth.* **199**, 531.

Ro83 Rogers D. W. O., 1983, "Use of EGS with Low Energy Electrons", National Research Council of Canada, Ottawa, to be published.

Ro83b Rogers, D. W. O., Bielajew, A. F., 1983, "The use of EGS for Radiation Dosimetry Problem", National Research Council of Canada, Ottawa, to be published.

St70 Storm E. and Israel H. I., 1970, "Photon Cross Sections from 1 keV to 100 MeV for Elements $Z = 1$ to $Z = 100$", *At. Data and Nucl. Data Tables* 7, 565.

Ta80 Tapia C. S. and Trubey D. K., 1980, "A Monte Carlo Calculation of Flux-to-Dose-Rate Conversion Factors for Energies between 0.01 and 1.00 MeV", Oak Ridge National Laboratory, Oak Ridge, TN, unpublished report.

APPENDIX A

This appendix presents tables of the dose equivalent per unit incident fluence as a function of depth for broad parallel beams of photons and electrons incident normally on a 30-cm-thick semi-infinite slab of ICRU four-element tissue. Different depth grids are used to present adequate detail of the shapes of the curves. Depths are given in centimeters and refer to the back edge of the bin. Values of dose-equivalent per unit incident fluence are given in $Sv \cdot cm^2$. Statistical uncertainties on each value are presented in brackets following the value. The uncertainties are rounded to the nearest percent and values $\geqslant 10\%$ are shown as $a*$. Generally, the systematic uncertainties discussed in the text are larger than these statistical uncertainties.

It is often useful to have similar conversion coefficients for a water phantom. For photons with energies between 1 and 20 MeV, these can be deduced

Tables 8–21. Dose equivalent (or absorbed dose to tissue) per unit incident fluence in $Sv \cdot cm^2$ for broad parallel beams incident normally on a 30-cm-thick semi-infinite slab of ICRU four-element tissue

Table 8.

Incident Photons

11. keV		15. keV		20.keV	
Depth	Sv x cm**2	Depth	Sv x cm**2	Depth	Sv x cm**2
0.01	5.40E-12(1)	0.01	2.97E-12(1)	0.05	1.68E-12(0)
0.02	5.23E-12(1)	0.02	2.86E-12(1)	0.10	1.68E-12(0)
0.03	5.19E-12(1)	0.03	2.88E-12(1)	0.15	1.60E-12(0)
0.04	4.87E-12(1)	0.04	2.91E-12(1)	0.20	1.59E-12(0)
0.08	4.59E-12(1)	0.05	2.83E-12(1)	0.25	1.57E-12(1)
0.12	4.10E-12(1)	0.10	2.72E-12(1)	0.30	1.51E-12(1)
0.16	3.52E-12(0)	0.15	2.57E-12(0)	0.35	1.47E-12(0)
0.20	3.06E-12(1)	0.20	2.41E-12(0)	0.40	1.43E-12(0)
0.24	2.67E-12(1)	0.25	2.27E-12(0)	0.60	1.35E-12(0)
0.28	2.34E-12(1)	0.30	2.14E-12(0)	0.80	1.20E-12(0)
0.32	2.10E-12(1)	0.35	1.99E-12(0)	1.00	1.07E-12(0)
0.36	1.75E-12(1)	0.40	1.87E-12(0)	1.50	8.71E-13(0)
0.40	1.52E-12(1)	0.60	1.59E-12(0)	2.00	6.47E-13(0)
0.60	1.07E-12(0)	0.80	1.21E-12(0)	2.50	4.74E-13(0)
0.80	5.28E-13(1)	1.00	9.14E-13(0)	3.00	3.43E-13(0)
1.00	2.71E-13(2)	1.50	5.79E-13(0)	3.50	2.51E-13(1)
1.20	1.41E-13(1)	2.00	2.89E-13(0)	4.00	1.83E-13(0)
1.40	7.19E-14(2)	2.50	1.48E-13(0)	4.50	1.29E-13(1)
1.60	3.52E-14(4)	3.00	7.42E-14(1)	5.00	9.32E-14(1)
1.80	1.80E-14(5)	3.50	3.73E-14(1)	6.00	5.98E-14(0)
2.00	9.15E-15(9)	4.00	1.81E-14(2)	7.00	3.05E-14(1)
3.00	0.00E-01(0)	4.50	8.75E-15(3)	8.00	1.57E-14(1)

from the present tables for ICRU tissue by using the conversion factors given in Table 22. The values in Table 22 are just the values of μ_{en}/ρ for water divided by those for tissue since, to first order, $D \alpha \mu_{en}/\rho$ (see equation (1) and Section 3.1.3) and in this energy region the ratio is close to unity.

Table 9.

	Incident Photons				
	30. keV	40. keV	50. keV	60. keV	80. keV
Depth	Sv x cm**2	Sv x cm**2	Sv x cm**2	Sv x cm**2	Sv x cm**2
0.20	8.83E-13(0)	6.36E-13(1)	5.21E-13(2)	5.17E-13(1)	5.70E-13(1)
0.40	8.69E-13(0)	6.36E-13(1)	5.32E-13(1)	5.46E-13(0)	5.85E-13(0)
0.60	8.46E-13(0)	6.41E-13(1)	5.62E-13(2)	5.50E-13(0)	6.00E-13(0)
0.80	8.37E-13(0)	6.47E-13(0)	5.78E-13(2)	5.64E-13(0)	6.15E-13(0)
1.00	8.16E-13(1)	6.55E-13(0)	5.86E-13(1)	5.55E-13(0)	6.18E-13(1)
1.50	7.64E-13(0)	6.33E-13(1)	5.73E-13(1)	5.64E-13(0)	6.25E-13(0)
2.00	6.90E-13(0)	6.15E-13(0)	5.68E-13(1)	5.76E-13(0)	6.27E-13(0)
2.50	6.27E-13(0)	5.86E-13(0)	5.70E-13(0)	5.60E-13(0)	6.23E-13(0)
3.00	5.56E-13(0)	5.57E-13(0)	5.55E-13(0)	5.62E-13(0)	6.25E-13(0)
3.50	4.96E-13(0)	5.23E-13(0)	5.28E-13(1)	5.48E-13(0)	6.20E-13(0)
4.00	4.40E-13(0)	4.94E-13(0)	5.16E-13(1)	5.27E-13(0)	6.14E-13(0)
4.50	3.92E-13(0)	4.61E-13(0)	4.90E-13(1)	5.24E-13(0)	5.98E-13(0)
5.00	3.40E-13(0)	4.29E-13(0)	4.77E-13(1)	4.97E-13(0)	5.83E-13(0)
6.00	2.84E-13(0)	3.88E-13(0)	4.31E-13(1)	4.70E-13(0)	5.55E-13(0)
7.00	2.16E-13(0)	3.29E-13(0)	3.83E-13(1)	4.32E-13(0)	5.22E-13(0)
8.00	1.65E-13(0)	2.79E-13(0)	3.48E-13(1)	3.96E-13(0)	4.90E-13(0)
9.00	1.25E-13(0)	2.36E-13(0)	2.99E-13(1)	3.60E-13(0)	4.56E-13(0)
10.00	9.51E-14(0)	1.96E-13(1)	2.71E-13(1)	3.28E-13(0)	4.19E-13(0)
15.00	4.40E-14(0)	1.20E-13(0)	1.82E-13(0)	2.35E-13(0)	3.24E-13(0)
20.00	1.02E-14(1)	4.70E-14(0)	8.93E-14(1)	1.26E-13(0)	1.96E-13(0)
25.00	2.08E-15(2)	1.73E-14(1)	4.18E-14(1)	6.38E-14(0)	1.09E-13(0)
30.00	4.82E-16(4)	5.82E-15(1)	1.62E-14(3)	2.73E-14(1)	5.11E-14(0)

Table 10.

	Incident Photons				
	100. keV	200. keV	300. keV	400. keV	500. keV
Depth	Sv x cm**2	Sv x cm**2	Sv x cm**2	Sv x cm**2	Sv x cm**2
0.20	6.57E-13(1)	1.29E-12(0)	1.94E-12(0)	2.46E-12(1)	2.85E-12(1)
0.40	6.90E-13(0)	1.33E-12(1)	1.97E-12(1)	2.60E-12(0)	3.09E-12(1)
0.60	6.94E-13(1)	1.35E-12(0)	1.99E-12(0)	2.62E-12(1)	3.12E-12(1)
0.80	7.13E-13(0)	1.36E-12(1)	1.99E-12(1)	2.58E-12(0)	3.17E-12(0)
1.00	7.20E-13(0)	1.39E-12(0)	1.99E-12(0)	2.63E-12(1)	3.18E-12(1)
1.50	7.26E-13(0)	1.38E-12(0)	2.03E-12(0)	2.61E-12(0)	3.15E-12(0)
2.00	7.33E-13(0)	1.38E-12(0)	2.01E-12(0)	2.61E-12(0)	3.18E-12(0)
2.50	7.31E-13(0)	1.37E-12(0)	2.00E-12(0)	2.59E-12(0)	3.13E-12(0)
3.00	7.30E-13(0)	1.36E-12(0)	2.02E-12(0)	2.57E-12(0)	3.11E-12(0)
3.50	7.25E-13(0)	1.35E-12(0)	1.97E-12(0)	2.56E-12(0)	3.10E-12(0)
4.00	7.18E-13(0)	1.33E-12(0)	1.96E-12(0)	2.52E-12(0)	3.05E-12(1)
4.50	6.99E-13(0)	1.32E-12(0)	1.92E-12(0)	2.50E-12(0)	3.01E-12(0)
5.00	6.85E-13(0)	1.30E-12(0)	1.90E-12(0)	2.46E-12(0)	2.97E-12(0)
6.00	6.66E-13(0)	1.26E-12(0)	1.83E-12(0)	2.40E-12(0)	2.88E-12(0)
7.00	6.25E-13(0)	1.20E-12(0)	1.76E-12(0)	2.31E-12(0)	2.78E-12(0)
8.00	5.95E-13(0)	1.15E-12(0)	1.70E-12(0)	2.22E-12(0)	2.69E-12(0)
9.00	5.49E-13(0)	1.08E-12(0)	1.63E-12(0)	2.12E-12(0)	2.60E-12(0)
10.00	5.14E-13(0)	1.02E-12(0)	1.54E-12(0)	2.04E-12(0)	2.49E-12(0)
15.00	4.08E-13(0)	8.49E-13(0)	1.30E-12(0)	1.75E-12(0)	2.17E-12(0)
20.00	2.60E-13(0)	5.91E-13(0)	9.45E-13(0)	1.31E-12(0)	1.68E-12(0)
25.00	1.53E-13(0)	3.85E-13(0)	6.44E-13(0)	9.33E-13(0)	1.22E-12(0)
30.00	7.49E-14(0)	2.15E-13(0)	3.91E-13(0)	5.93E-13(0)	8.14E-13(0)

Table 11.

	Incident Photons					
	600. keV	800. keV	1000. keV	1250. keV	2000. keV	3000. keV
Depth	Sv x cm**2	Sv x cm**2	Sv x cm**2	Sv x cm**2	Sv x cm**2	Sv x cm**2
0.20	3.15E-12(0)	3.73E-12(1)	3.80E-12(1)	3.53E-12(0)	2.70E-12(1)	2.10E-12(1)
0.40	3.59E-12(0)	4.54E-12(1)	5.38E-12(0)	6.25E-12(0)	6.29E-12(0)	5.13E-12(0)
0.60	3.61E-12(1)	4.57E-12(0)	5.44E-12(0)	6.42E-12(0)	8.35E-12(0)	7.81E-12(0)
0.80	3.63E-12(1)	4.63E-12(1)	5.46E-12(0)	6.35E-12(0)	8.63E-12(0)	9.81E-12(0)
1.00	3.62E-12(1)	4.66E-12(1)	5.49E-12(0)	6.36E-12(0)	8.64E-12(0)	1.10E-11(0)
1.50	3.64E-12(0)	4.56E-12(1)	5.47E-12(0)	6.37E-12(0)	8.73E-12(0)	1.13E-11(0)
2.00	3.65E-12(0)	4.66E-12(0)	5.36E-12(0)	6.35E-12(0)	8.66E-12(0)	1.12E-11(0)
2.50	3.62E-12(1)	4.49E-12(0)	5.39E-12(0)	6.22E-12(0)	8.51E-12(0)	1.10E-11(0)
3.00	3.60E-12(0)	4.54E-12(0)	5.34E-12(0)	6.23E-12(0)	8.46E-12(0)	1.09E-11(0)
3.50	3.59E-12(0)	4.45E-12(0)	5.30E-12(1)	6.11E-12(0)	8.41E-12(0)	1.09E-11(0)
4.00	3.56E-12(0)	4.45E-12(0)	5.14E-12(0)	6.12E-12(0)	8.29E-12(0)	1.09E-11(0)
4.50	3.48E-12(0)	4.38E-12(0)	5.18E-12(1)	6.09E-12(0)	8.35E-12(0)	1.08E-11(0)
5.00	3.42E-12(0)	4.29E-12(0)	5.12E-12(0)	5.96E-12(0)	8.30E-12(0)	1.07E-11(0)
6.00	3.39E-12(0)	4.24E-12(0)	5.02E-12(0)	5.82E-12(0)	8.09E-12(0)	1.06E-11(0)
7.00	3.27E-12(0)	4.09E-12(0)	4.91E-12(0)	5.79E-12(0)	7.93E-12(0)	1.03E-11(0)
8.00	3.18E-12(0)	3.99E-12(0)	4.82E-12(0)	5.59E-12(0)	7.89E-12(0)	1.02E-11(0)
9.00	3.06E-12(0)	3.89E-12(0)	4.64E-12(0)	5.41E-12(0)	7.52E-12(0)	1.01E-11(0)
10.00	2.93E-12(0)	3.75E-12(0)	4.51E-12(0)	5.32E-12(0)	7.43E-12(0)	1.00E-11(1)
15.00	2.58E-12(0)	3.35E-12(0)	4.03E-12(0)	4.80E-12(0)	6.91E-12(0)	9.21E-12(0)
20.00	2.02E-12(0)	2.69E-12(0)	3.35E-12(1)	4.10E-12(1)	5.99E-12(1)	8.34E-12(0)
25.00	1.51E-12(0)	2.09E-12(0)	2.60E-12(1)	3.37E-12(1)	5.18E-12(1)	7.33E-12(0)
30.00	1.05E-12(0)	1.52E-12(0)	2.03E-12(3)	2.66E-12(2)	4.20E-12(2)	6.17E-12(1)

Table 12.

	Incident Photons					
	4. MeV	5. MeV	6. MeV	7. MeV	8. MeV	10. MeV
Depth	Sv x cm**2	Sv x cm**2	Sv x cm**2	Sv x cm**2	Sv x cm**2	Sv x cm**2
0.20	1.79E-12(1)	1.61E-12(0)	1.45E-12(1)	1.42E-12(1)	1.34E-12(1)	1.37E-12(3)
0.40	4.37E-12(0)	3.97E-12(1)	3.68E-12(0)	3.48E-12(0)	3.29E-12(1)	3.11E-12(2)
0.60	6.85E-12(0)	6.17E-12(1)	5.77E-12(0)	5.47E-12(0)	5.18E-12(0)	4.87E-12(3)
0.80	9.15E-12(0)	8.33E-12(0)	7.81E-12(0)	7.46E-12(0)	7.03E-12(0)	6.69E-12(2)
1.00	1.09E-11(0)	1.02E-11(0)	9.77E-12(0)	9.23E-12(0)	8.82E-12(0)	8.50E-12(2)
1.50	1.29E-11(0)	1.31E-11(0)	1.26E-11(0)	1.23E-11(0)	1.18E-11(0)	1.14E-11(1)
2.00	1.35E-11(0)	1.53E-11(0)	1.57E-11(0)	1.58E-11(0)	1.54E-11(0)	1.50E-11(1)
2.50	1.33E-11(0)	1.55E-11(0)	1.70E-11(0)	1.82E-11(0)	1.82E-11(0)	1.81E-11(1)
3.00	1.32E-11(0)	1.52E-11(0)	1.72E-11(0)	1.91E-11(0)	2.00E-11(0)	2.07E-11(0)
3.50	1.32E-11(0)	1.51E-11(0)	1.73E-11(0)	1.91E-11(0)	2.09E-11(0)	2.28E-11(0)
4.00	1.29E-11(0)	1.50E-11(0)	1.72E-11(0)	1.91E-11(0)	2.10E-11(0)	2.39E-11(0)
4.50	1.29E-11(0)	1.49E-11(0)	1.70E-11(0)	1.90E-11(0)	2.08E-11(0)	2.43E-11(0)
5.00	1.28E-11(0)	1.48E-11(0)	1.69E-11(0)	1.88E-11(0)	2.07E-11(0)	2.39E-11(0)
6.00	1.27E-11(0)	1.48E-11(0)	1.66E-11(0)	1.86E-11(0)	2.05E-11(0)	2.41E-11(0)
7.00	1.26E-11(0)	1.45E-11(0)	1.64E-11(0)	1.84E-11(0)	2.02E-11(0)	2.38E-11(0)
8.00	1.22E-11(0)	1.43E-11(0)	1.62E-11(0)	1.81E-11(0)	2.01E-11(0)	2.36E-11(1)
9.00	1.20E-11(0)	1.41E-11(0)	1.60E-11(0)	1.80E-11(0)	1.98E-11(0)	2.33E-11(1)
10.00	1.21E-11(0)	1.38E-11(0)	1.56E-11(0)	1.76E-11(0)	1.97E-11(0)	2.32E-11(1)
15.00	1.13E-11(0)	1.32E-11(0)	1.51E-11(0)	1.68E-11(0)	1.87E-11(0)	2.20E-11(0)
20.00	1.03E-11(0)	1.21E-11(0)	1.38E-11(0)	1.55E-11(0)	1.72E-11(0)	2.09E-11(0)
25.00	9.21E-12(0)	1.11E-11(0)	1.25E-11(0)	1.43E-11(0)	1.58E-11(0)	1.93E-11(1)
30.00	8.02E-12(0)	9.78E-12(1)	1.13E-11(0)	1.28E-11(0)	1.42E-11(0)	1.79E-11(1)

Table 13.

	Incident Photons					
	20. MeV	30. MeV	40. MeV	50. MeV	100. MeV	200. MeV
Depth	Sv x cm**2	Sv x cm**2	Sv x cm**2	Sv x cm**2	Sv x cm**2	Sv x cm**2
0.20	1.24E-12(2)	1.22E-12(6)	1.28E-12(5)	1.24E-12(8)	1.22E-12(*)	1.57E-12(*)
0.40	2.82E-12(2)	2.77E-12(2)	3.03E-12(4)	3.03E-12(6)	3.16E-12(7)	3.43E-12(7)
0.60	4.37E-12(1)	4.33E-12(3)	4.70E-12(4)	4.77E-12(4)	5.34E-12(6)	5.15E-12(8)
0.80	5.96E-12(1)	6.05E-12(2)	6.70E-12(4)	6.78E-12(3)	7.37E-12(4)	7.59E-12(5)
1.00	7.82E-12(1)	7.81E-12(2)	8.15E-12(2)	8.59E-12(2)	9.28E-12(4)	9.92E-12(5)
2.00	1.23E-11(0)	1.24E-11(1)	1.34E-11(2)	1.40E-11(2)	1.50E-11(2)	1.66E-11(3)
3.00	1.96E-11(0)	2.04E-11(1)	2.18E-11(1)	2.29E-11(1)	2.51E-11(1)	2.69E-11(3)
4.00	2.61E-11(0)	2.81E-11(1)	2.93E-11(1)	3.13E-11(0)	3.48E-11(1)	3.63E-11(3)
5.00	3.13E-11(0)	3.46E-11(1)	3.65E-11(1)	3.95E-11(1)	4.43E-11(1)	4.76E-11(3)
6.00	3.56E-11(0)	3.97E-11(1)	4.30E-11(1)	4.65E-11(1)	5.32E-11(1)	5.89E-11(3)
8.00	3.96E-11(0)	4.62E-11(0)	5.11E-11(0)	5.70E-11(0)	6.59E-11(2)	7.54E-11(2)
10.00	4.16E-11(0)	5.31E-11(1)	6.05E-11(0)	6.85E-11(0)	8.14E-11(1)	9.56E-11(2)
12.00	4.08E-11(0)	5.69E-11(0)	6.75E-11(0)	7.74E-11(0)	9.58E-11(2)	1.15E-10(1)
14.00	3.99E-11(0)	5.77E-11(0)	7.17E-11(0)	8.48E-11(0)	1.10E-10(1)	1.34E-10(1)
16.00	3.97E-11(0)	5.69E-11(0)	7.32E-11(0)	8.93E-11(0)	1.22E-10(1)	1.50E-10(1)
18.00	3.82E-11(0)	5.53E-11(0)	7.25E-11(0)	9.18E-11(0)	1.32E-10(1)	1.64E-10(2)
20.00	3.73E-11(0)	5.41E-11(0)	7.14E-11(0)	9.25E-11(0)	1.41E-10(1)	1.77E-10(1)
22.00	3.56E-11(0)	5.26E-11(0)	6.97E-11(0)	9.13E-11(1)	1.44E-10(1)	1.89E-10(1)
24.00	3.44E-11(0)	5.15E-11(0)	6.77E-11(1)	8.89E-11(1)	1.49E-10(1)	2.00E-10(1)
26.00	3.35E-11(1)	5.01E-11(0)	6.57E-11(1)	8.62E-11(0)	1.53E-10(1)	2.11E-10(1)
28.00	3.27E-11(1)	4.84E-11(0)	6.50E-11(1)	8.26E-11(0)	1.52E-10(1)	2.18E-10(1)
29.50	3.18E-11(1)	4.75E-11(1)	6.35E-11(0)	8.06E-11(0)	1.52E-10(1)	2.25E-10(1)
30.00	3.12E-11(1)	4.67E-11(1)	6.27E-11(0)	7.85E-11(0)	1.51E-10(0)	2.27E-10(1)

Table 14.

	Incident Photons					
	500. MeV	1000. MeV	2000. MeV	5000. MeV	10000. MeV	20000. MeV
Depth	Sv x cm**2	Sv x cm**2	Sv x cm**2	Sv x cm**2	Sv x cm**2	Sv x cm**2
0.20	1.28E-12(9)	1.56E-12(*)	1.45E-12(*)	1.53E-12(*)	1.23E-12(*)	1.35E-12(*)
0.40	3.57E-12(6)	3.91E-12(*)	4.24E-12(*)	4.62E-12(8)	2.99E-12(*)	3.81E-12(*)
0.60	6.27E-12(5)	5.08E-12(*)	6.48E-12(*)	7.46E-12(6)	4.95E-12(*)	6.51E-12(*)
0.80	8.73E-12(6)	8.89E-12(*)	8.81E-12(7)	1.02E-11(6)	6.51E-12(*)	9.72E-12(*)
1.00	1.14E-11(4)	1.18E-11(*)	1.08E-11(7)	1.31E-11(8)	8.99E-12(*)	1.19E-11(*)
2.00	1.83E-11(2)	1.96E-11(6)	1.85E-11(6)	2.09E-11(6)	1.64E-11(9)	1.89E-11(*)
3.00	2.87E-11(3)	3.17E-11(7)	3.02E-11(3)	3.61E-11(4)	2.95E-11(8)	3.11E-11(6)
4.00	3.92E-11(3)	4.33E-11(5)	4.43E-11(4)	4.92E-11(4)	4.43E-11(5)	4.59E-11(4)
5.00	5.02E-11(2)	5.50E-11(4)	6.14E-11(4)	6.45E-11(3)	5.89E-11(2)	5.86E-11(4)
6.00	6.13E-11(2)	6.73E-11(3)	7.46E-11(4)	7.84E-11(3)	7.37E-11(3)	7.26E-11(4)
8.00	7.71E-11(2)	8.72E-11(3)	9.14E-11(4)	9.98E-11(3)	9.42E-11(3)	9.33E-11(3)
10.00	1.00E-10(1)	1.10E-10(2)	1.16E-10(3)	1.29E-10(3)	1.25E-10(2)	1.24E-10(2)
12.00	1.23E-10(1)	1.38E-10(2)	1.41E-10(2)	1.63E-10(3)	1.57E-10(2)	1.58E-10(2)
14.00	1.45E-10(1)	1.64E-10(3)	1.70E-10(2)	1.91E-10(3)	1.92E-10(1)	1.94E-10(2)
16.00	1.66E-10(1)	1.88E-10(2)	1.94E-10(2)	2.27E-10(3)	2.27E-10(1)	2.29E-10(2)
18.00	1.91E-10(1)	2.14E-10(2)	2.23E-10(2)	2.60E-10(3)	2.66E-10(2)	2.74E-10(1)
20.00	2.12E-10(1)	2.40E-10(2)	2.53E-10(2)	2.95E-10(2)	3.04E-10(1)	3.15E-10(1)
22.00	2.34E-10(1)	2.66E-10(2)	2.84E-10(2)	3.31E-10(2)	3.49E-10(1)	3.64E-10(1)
24.00	2.53E-10(1)	2.95E-10(2)	3.13E-10(1)	3.74E-10(2)	3.96E-10(1)	4.19E-10(1)
26.00	2.76E-10(1)	3.24E-10(2)	3.47E-10(1)	4.16E-10(1)	4.44E-10(2)	4.76E-10(1)
28.00	2.92E-10(1)	3.45E-10(2)	3.86E-10(1)	4.64E-10(1)	4.97E-10(1)	5.26E-10(1)
29.50	3.11E-10(0)	3.66E-10(2)	4.21E-10(1)	5.01E-10(1)	5.45E-10(1)	5.86E-10(1)
30.00	3.18E-10(0)	3.79E-10(2)	4.35E-10(1)	5.21E-10(1)	5.77E-10(1)	6.19E-10(1)

Table 15.

Incident Electrons

100. keV		200. keV		300. keV		400. keV	
Depth	Sv x cm**2	Depth	Sv x cm**2	Depth	Sv x cm**2	Depth	Sv x cm**2
0.001	9.11E-10(0)	0.002	5.64E-10(0)	0.005	4.79E-10(0)	0.008	4.32E-10(0)
0.002	1.17E-09(1)	0.005	7.02E-10(0)	0.010	5.95E-10(1)	0.016	5.20E-10(1)
0.003	1.46E-09(1)	0.008	8.65E-10(1)	0.015	7.01E-10(1)	0.024	6.18E-10(0)
0.004	1.66E-09(0)	0.011	1.01E-09(1)	0.020	6.21E-10(1)	0.032	7.35E-10(1)
0.005	1.86E-09(0)	0.014	1.16E-09(0)	0.025	8.99E-10(0)	0.040	8.08E-10(1)
0.006	1.92E-09(0)	0.017	1.23E-09(1)	0.030	9.55E-10(1)	0.048	8.22E-10(1)
0.007	1.85E-09(1)	0.020	1.19E-09(1)	0.035	9.66E-10(1)	0.056	8.29E-10(0)
0.008	1.67E-09(1)	0.023	1.09E-09(1)	0.040	9.22E-10(1)	0.064	7.92E-10(1)
0.009	1.34E-09(0)	0.026	9.92E-10(1)	0.045	8.37E-10(1)	0.072	7.01E-10(1)
0.010	1.03E-09(1)	0.029	7.90E-10(1)	0.050	7.32E-10(1)	0.080	5.93E-10(1)
0.011	6.10E-10(2)	0.032	5.46E-10(1)	0.055	5.98E-10(2)	0.088	4.54E-10(2)
0.012	2.33E-10(4)	0.035	3.34E-10(2)	0.060	4.56E-10(1)	0.096	3.05E-10(1)
0.013	2.08E-11(*)	0.038	1.40E-10(4)	0.065	2.76E-10(1)	0.104	1.70E-10(2)
0.014	0.00E+00(0)	0.041	3.08E-11(7)	0.070	1.49E-10(3)	0.112	7.22E-11(5)
0.015	0.00E+00(0)	0.044	1.19E-12(*)	0.075	5.05E-11(5)	0.120	1.76E-11(6)
0.065	0.00E+00(0)	0.047	0.00E+00(0)	0.080	6.69E-12(*)	0.128	1.64E-12(*)
0.145	0.00E+00(0)	0.050	0.00E+00(0)	0.085	1.86E-13(*)	0.136	0.00E+00(0)
0.245	0.00E+00(0)	0.100	0.00E+00(0)	0.090	4.80E-14(*)	0.144	0.00E+00(0)

Table 16.

Incident Electrons

500. keV			600. keV	700. keV		800. keV	900. keV
Depth	Sv x cm**2	Depth	Sv x cm**2	Sv x cm**2	Depth	Sv x cm**2	Sv x cm**2
0.010	3.92E-10(1)	0.015	3.89E-10(0)	3.57E-10(0)	0.02	3.50E-10(0)	3.38E-10(0)
0.020	4.72E-10(1)	0.030	4.59E-10(0)	4.16E-10(0)	0.04	4.14E-10(0)	3.90E-10(1)
0.030	5.41E-10(1)	0.045	5.52E-10(0)	4.82E-10(1)	0.06	4.90E-10(1)	4.43E-10(1)
0.040	6.33E-10(1)	0.060	6.34E-10(1)	5.61E-10(0)	0.08	5.60E-10(0)	5.08E-10(1)
0.050	7.18E-10(1)	0.075	6.95E-10(1)	6.15E-10(1)	0.10	6.19E-10(1)	5.60E-10(0)
0.060	7.68E-10(1)	0.090	7.16E-10(1)	6.52E-10(1)	0.12	6.48E-10(1)	6.03E-10(0)
0.070	7.59E-10(1)	0.105	6.90E-10(1)	6.63E-10(0)	0.14	6.44E-10(1)	6.35E-10(1)
0.080	7.44E-10(1)	0.120	6.31E-10(1)	6.57E-10(1)	0.16	6.14E-10(0)	6.29E-10(1)
0.090	6.91E-10(1)	0.135	5.44E-10(1)	6.41E-10(0)	0.18	5.61E-10(1)	5.92E-10(1)
0.100	6.34E-10(1)	0.150	4.29E-10(1)	5.88E-10(0)	0.20	4.85E-10(1)	5.59E-10(1)
0.110	5.30E-10(1)	0.165	2.99E-10(2)	5.10E-10(1)	0.22	3.80E-10(1)	4.93E-10(1)
0.120	4.05E-10(2)	0.180	1.71E-10(2)	4.37E-10(1)	0.24	2.71E-10(2)	4.31E-10(1)
0.130	2.87E-10(2)	0.195	7.24E-11(3)	3.27E-10(1)	0.26	1.67E-10(1)	3.41E-10(1)
0.140	1.77E-10(2)	0.210	2.18E-11(6)	2.27E-10(2)	0.28	7.72E-11(2)	2.59E-10(2)
0.150	8.87E-11(4)	0.225	2.60E-12(*)	1.35E-10(1)	0.30	2.82E-11(4)	1.66E-10(2)
0.160	3.17E-11(9)	0.240	7.11E-14(*)	6.43E-11(2)	0.32	5.42E-12(*)	9.70E-11(3)
0.170	5.85E-12(*)	0.255	4.06E-14(*)	2.14E-11(8)	0.34	4.06E-13(*)	3.78E-11(5)
0.180	2.80E-13(*)	0.270	3.17E-14(*)	3.95E-12(*)	0.36	1.34E-13(*)	1.20E-11(*)
0.190	1.89E-14(*)	0.285	2.45E-15(*)	3.97E-13(*)	0.38	2.99E-14(*)	1.56E-12(*)
0.200	0.00E+00(0)	0.300	1.05E-13(*)	9.26E-14(*)	0.40	2.40E-14(*)	2.38E-13(*)

Table 17.

Incident Electrons					
1.0 MeV		1.5 MeV		2.0 MeV	
Depth	Sv x cm**2	Depth	Sv x cm**2	Depth	Sv x cm**2
0.025	3.40E-10(0)	0.050	3.26E-10(0)	0.050	3.14E-10(0)
0.050	3.84E-10(1)	0.100	3.77E-10(0)	0.100	3.43E-10(0)
0.075	4.48E-10(1)	0.150	4.36E-10(1)	0.150	3.78E-10(0)
0.100	5.15E-10(1)	0.200	4.99E-10(1)	0.200	4.11E-10(1)
0.125	5.68E-10(1)	0.250	5.45E-10(0)	0.250	4.58E-10(1)
0.150	6.12E-10(0)	0.300	5.59E-10(0)	0.300	4.94E-10(0)
0.175	6.15E-10(1)	0.350	5.44E-10(1)	0.350	5.30E-10(1)
0.200	5.92E-10(0)	0.400	4.79E-10(0)	0.400	5.33E-10(1)
0.225	5.45E-10(1)	0.450	3.90E-10(1)	0.450	5.19E-10(0)
0.250	5.03E-10(1)	0.500	2.97E-10(1)	0.500	5.04E-10(0)
0.275	4.27E-10(1)	0.550	1.82E-10(1)	0.550	4.56E-10(0)
0.300	3.33E-10(2)	0.600	8.35E-11(3)	0.600	4.12E-10(1)
0.325	2.24E-10(2)	0.650	2.06E-11(4)	0.650	3.36E-10(1)
0.350	1.38E-10(3)	0.700	3.10E-12(*)	0.700	2.65E-10(1)
0.375	6.32E-11(6)	0.750	1.84E-13(*)	0.750	1.76E-10(1)
0.400	1.27E-11(9)	0.800	6.00E-14(*)	0.800	1.14E-10(2)
0.425	9.10E-13(*)	0.850	1.30E-13(*)	0.850	5.17E-11(4)
0.450	2.00E-14(*)	0.900	1.00E-13(*)	0.900	1.66E-11(8)
0.475	6.80E-14(*)	1.000	7.80E-14(*)	1.000	2.30E-12(*)
0.500	8.30E-14(*)	1.500	1.29E-13(*)	1.500	1.70E-13(*)
1.000	4.00E-14(*)	2.000	9.00E-14(*)	2.000	1.67E-13(*)

Table 18.

Incident Electrons						
	3. MeV	4. MeV	5. MeV		7. MeV	10. MeV
Depth	Sv x cm**2	Sv x cm**2	Sv x cm**2	Depth	Sv x cm**2	Sv x cm**2
0.10	3.13E-10(0)	3.00E-10(0)	2.95E-10(0)	0.10	2.92E-10(0)	2.89E-10(0)
0.20	3.43E-10(0)	3.22E-10(0)	3.11E-10(0)	0.20	3.08E-10(0)	3.01E-10(0)
0.30	3.78E-10(0)	3.43E-10(0)	3.27E-10(0)	0.30	3.15E-10(0)	3.06E-10(0)
0.40	4.16E-10(0)	3.62E-10(0)	3.39E-10(0)	0.40	3.19E-10(0)	3.11E-10(0)
0.50	4.58E-10(0)	3.87E-10(0)	3.55E-10(0)	0.60	3.29E-10(0)	3.20E-10(0)
0.60	4.95E-10(0)	4.18E-10(0)	3.71E-10(0)	0.80	3.42E-10(0)	3.27E-10(0)
0.70	5.00E-10(0)	4.39E-10(0)	3.88E-10(0)	1.00	3.60E-10(0)	3.35E-10(0)
0.80	4.79E-10(0)	4.66E-10(0)	4.01E-10(0)	1.25	3.85E-10(0)	3.42E-10(0)
0.90	4.29E-10(0)	4.77E-10(1)	4.20E-10(0)	1.50	4.14E-10(0)	3.57E-10(0)
1.00	3.61E-10(1)	4.73E-10(0)	4.37E-10(1)	1.75	4.36E-10(0)	3.67E-10(0)
1.10	2.66E-10(1)	4.62E-10(1)	4.53E-10(0)	2.00	4.41E-10(0)	3.78E-10(0)
1.20	1.73E-10(1)	4.46E-10(1)	4.74E-10(0)	2.25	4.17E-10(0)	3.94E-10(0)
1.30	8.41E-11(2)	3.86E-10(1)	4.66E-10(1)	2.50	3.69E-10(0)	4.07E-10(0)
1.40	2.76E-11(3)	3.26E-10(0)	4.66E-10(0)	2.75	2.81E-10(1)	4.15E-10(0)
1.50	4.59E-12(*)	2.69E-10(1)	4.42E-10(0)	3.00	1.79E-10(1)	4.17E-10(0)
1.60	7.20E-13(*)	1.96E-10(2)	4.05E-10(0)	3.25	8.55E-11(2)	4.01E-10(0)
1.80	3.46E-13(*)	9.34E-11(2)	3.47E-10(1)	3.50	2.66E-11(4)	3.76E-10(1)
2.00	1.48E-13(*)	1.59E-11(4)	2.33E-10(1)	4.00	2.42E-12(6)	3.01E-10(0)
2.20	2.70E-13(*)	9.14E-13(*)	1.22E-10(1)	4.50	1.24E-12(*)	1.63E-10(1)
2.40	4.54E-13(*)	6.57E-13(*)	4.18E-11(3)	5.00	1.26E-12(*)	4.68E-11(3)
2.80	2.65E-13(*)	3.60E-13(*)	3.28E-12(6)	5.50	1.08E-12(*)	5.15E-12(7)
3.20	1.76E-13(*)	2.86E-13(*)	6.30E-13(*)	6.50	9.54E-13(*)	2.29E-12(6)

Table 19.

Depth	Incident Electrons 20. MeV Sv x cm**2	Depth	30. MeV Sv x cm**2	40. MeV Sv x cm**2	50. MeV Sv x cm**2
0.10	2.96E-10(0)	0.10	2.96E-10(0)	2.96E-10(0)	2.97E-10(0)
0.20	3.01E-10(0)	0.20	3.01E-10(0)	3.01E-10(0)	3.02E-10(0)
0.30	3.05E-10(0)	0.30	3.06E-10(0)	3.03E-10(0)	3.06E-10(0)
0.40	3.08E-10(0)	0.40	3.08E-10(0)	3.07E-10(0)	3.08E-10(0)
0.60	3.11E-10(0)	0.60	3.12E-10(0)	3.13E-10(0)	3.14E-10(0)
0.80	3.20E-10(0)	0.80	3.16E-10(0)	3.15E-10(0)	3.16E-10(0)
1.00	3.24E-10(0)	1.00	3.20E-10(0)	3.21E-10(0)	3.18E-10(0)
1.50	3.26E-10(0)	3.00	3.31E-10(0)	3.31E-10(0)	3.30E-10(0)
2.00	3.34E-10(0)	5.00	3.47E-10(0)	3.43E-10(0)	3.41E-10(0)
2.50	3.40E-10(0)	7.00	3.53E-10(0)	3.49E-10(0)	3.47E-10(0)
3.00	3.46E-10(0)	9.00	3.53E-10(0)	3.49E-10(0)	3.51E-10(0)
3.50	3.51E-10(0)	11.00	3.21E-10(0)	3.42E-10(0)	3.52E-10(0)
4.00	3.56E-10(0)	13.00	2.20E-10(1)	3.24E-10(0)	3.42E-10(0)
5.00	3.63E-10(0)	15.00	7.59E-11(2)	2.80E-10(0)	3.27E-10(0)
6.00	3.65E-10(0)	17.00	1.20E-11(4)	1.99E-10(0)	2.97E-10(0)
7.00	3.50E-10(0)	19.00	1.09E-11(5)	9.51E-11(1)	2.47E-10(0)
8.00	2.94E-10(0)	21.00	9.82E-12(5)	2.90E-11(2)	1.74E-10(1)
9.00	1.88E-10(1)	23.00	8.82E-12(3)	1.72E-11(4)	9.88E-11(1)
10.00	6.50E-11(1)	25.00	9.17E-12(4)	1.62E-11(4)	4.43E-11(2)
11.00	7.24E-12(5)	27.00	8.83E-12(3)	1.51E-11(4)	2.47E-11(3)
12.00	5.97E-12(4)	29.00	8.22E-12(4)	1.34E-11(4)	2.28E-11(3)
13.00	6.01E-12(5)	30.00	7.69E-12(4)	1.23E-11(4)	2.11E-11(4)

Table 20.

Depth	Incident Electrons 70. MeV Sv x cm**2	100. MeV Sv x cm**2	200. MeV Sv x cm**2	500. MeV Sv x cm**2	1000. MeV Sv x cm**2
0.10	2.96E-10(0)	2.94E-10(0)	2.97E-10(0)	2.96E-10(0)	2.96E-10(0)
0.20	3.01E-10(0)	2.99E-10(0)	3.02E-10(0)	3.02E-10(0)	3.00E-10(0)
0.30	3.06E-10(0)	3.02E-10(0)	3.09E-10(0)	3.03E-10(0)	3.03E-10(0)
0.40	3.07E-10(0)	3.07E-10(0)	3.09E-10(0)	3.06E-10(0)	3.06E-10(0)
0.60	3.10E-10(0)	3.11E-10(0)	3.06E-10(0)	3.11E-10(0)	3.10E-10(0)
0.80	3.16E-10(0)	3.14E-10(0)	3.16E-10(0)	3.14E-10(0)	3.12E-10(0)
1.00	3.19E-10(0)	3.19E-10(0)	3.16E-10(0)	3.18E-10(0)	3.18E-10(0)
3.00	3.28E-10(0)	3.31E-10(0)	3.28E-10(0)	3.31E-10(0)	3.31E-10(0)
5.00	3.39E-10(0)	3.44E-10(0)	3.43E-10(0)	3.48E-10(0)	3.49E-10(0)
7.00	3.51E-10(0)	3.55E-10(0)	3.55E-10(0)	3.67E-10(1)	3.70E-10(0)
9.00	3.54E-10(0)	3.60E-10(0)	3.68E-10(0)	3.84E-10(0)	3.94E-10(1)
11.00	3.57E-10(0)	3.71E-10(0)	3.79E-10(0)	4.08E-10(0)	4.16E-10(0)
13.00	3.54E-10(0)	3.74E-10(0)	3.88E-10(0)	4.29E-10(0)	4.47E-10(0)
15.00	3.49E-10(0)	3.72E-10(0)	3.98E-10(0)	4.50E-10(0)	4.70E-10(1)
17.00	3.41E-10(0)	3.68E-10(0)	4.05E-10(0)	4.67E-10(1)	4.99E-10(1)
19.00	3.28E-10(0)	3.65E-10(0)	4.13E-10(0)	4.83E-10(1)	5.36E-10(1)
21.00	3.05E-10(0)	3.60E-10(0)	4.24E-10(0)	5.02E-10(0)	5.74E-10(1)
23.00	2.72E-10(0)	3.45E-10(0)	4.26E-10(1)	5.21E-10(0)	6.07E-10(1)
25.00	2.35E-10(1)	3.31E-10(0)	4.25E-10(1)	5.36E-10(1)	6.30E-10(1)
27.00	1.89E-10(1)	3.09E-10(1)	4.20E-10(1)	5.57E-10(1)	6.62E-10(1)
29.00	1.42E-10(1)	2.82E-10(1)	4.19E-10(1)	5.71E-10(1)	6.95E-10(1)
29.50	1.07E-10(1)	2.64E-10(1)	4.23E-10(1)	5.76E-10(1)	7.22E-10(1)
30.00	1.07E-10(1)	2.61E-10(1)	4.19E-10(1)	5.84E-10(1)	7.16E-10(1)

Table 21.

	Incident Electrons			
	2000. MeV	5000. MeV	10000. MeV	20000. MeV
Depth	Sv x cm**2	Sv x cm**2	Sv x cm**2	Sv x cm**2
0.10	2.98E-10(0)	2.94E-10(0)	2.96E-10(0)	2.96E-10(0)
0.20	3.02E-10(0)	3.00E-10(0)	3.00E-10(0)	3.00E-10(0)
0.30	3.05E-10(0)	3.06E-10(0)	3.05E-10(0)	3.03E-10(0)
0.40	3.05E-10(0)	3.11E-10(0)	3.11E-10(0)	3.08E-10(0)
0.60	3.12E-10(0)	3.14E-10(0)	3.12E-10(0)	3.14E-10(0)
0.80	3.18E-10(0)	3.18E-10(0)	3.16E-10(0)	3.17E-10(0)
1.00	3.21E-10(0)	3.22E-10(0)	3.21E-10(0)	3.21E-10(0)
3.00	3.31E-10(0)	3.35E-10(0)	3.35E-10(0)	3.36E-10(0)
5.00	3.50E-10(0)	3.59E-10(0)	3.61E-10(0)	3.63E-10(0)
7.00	3.76E-10(0)	3.85E-10(0)	3.91E-10(0)	4.00E-10(0)
9.00	4.03E-10(1)	4.18E-10(0)	4.34E-10(0)	4.45E-10(0)
11.00	4.38E-10(0)	4.58E-10(1)	4.79E-10(0)	5.03E-10(0)
13.00	4.69E-10(0)	5.03E-10(1)	5.33E-10(0)	5.66E-10(0)
15.00	5.04E-10(0)	5.49E-10(1)	5.89E-10(0)	6.31E-10(0)
17.00	5.41E-10(1)	6.05E-10(1)	6.55E-10(0)	7.01E-10(0)
19.00	5.84E-10(1)	6.53E-10(1)	7.25E-10(0)	7.85E-10(0)
21.00	6.30E-10(0)	7.13E-10(1)	7.93E-10(0)	8.73E-10(0)
23.00	6.71E-10(0)	7.81E-10(1)	8.78E-10(0)	9.75E-10(0)
25.00	7.15E-10(1)	8.49E-10(1)	9.65E-10(1)	1.08E-09(0)
27.00	7.59E-10(1)	9.10E-10(1)	1.05E-09(1)	1.19E-09(0)
29.00	8.11E-10(1)	9.84E-10(0)	1.14E-09(0)	1.30E-09(0)
29.50	8.46E-10(0)	1.03E-09(0)	1.20E-09(0)	1.38E-09(0)
30.00	8.47E-10(0)	1.03E-09(0)	1.21E-09(0)	1.41E-09(0)

Table 22. *To first order, conversion factors from fluence to absorbed dose to ICRU four-element tissues times the following factors give fluence to absorbed dose to water conversion factors. These values are taken from Hu*82

E_γ MeV	Conversion factor to water from tissue
0.015	1.086
0.020	1.086
0.030	1.083
0.040	1.073
0.050	1.059
0.060	1.045
0.080	1.026
0.100	1.018
0.150	1.011
0.200	1.010
0.300	1.010
0.400	1.010
0.500	1.010
0.600	1.010
0.800	1.009
1.0	1.009
1.5	1.010
2.0	1.010
3.0	1.010
4.0	1.011
5.0	1.011
6.0	1.012
8.0	1.012
10.0	1.014
15.0	1.015
20.0	1.016